

# A Semi-Bayesian Nonparametric Hypothesis Test Using Maximum Mean Discrepancy with Applications in Generative Adversarial Networks

**Forough Fazeli-Asl**

*Department of Statistics and Actuarial Science  
University of Hong Kong  
Pok Fu Lam, Hong Kong*

FOROUGHF@HKU.HK

**Michael Minyi Zhang**

*Department of Statistics and Actuarial Science  
University of Hong Kong  
Pok Fu Lam, Hong Kong*

MZHANG18@HKU.HK

**Lizhen Lin**

*Department of Applied and Computational Mathematics and Statistics  
University of Notre Dame  
South Bend, Indiana, USA*

LIZHEN.LIN@ND.EDU

## Abstract

A classic inferential problem in statistics is the two-sample hypothesis test, where we test whether two samples of observations are either drawn from the same distribution or two distinct distributions. However, standard methods for performing this test require strong distributional assumptions on the two samples of data. We propose a semi-Bayesian nonparametric (semi-BNP) procedure for the two-sample hypothesis testing problem. First, we will derive a novel BNP maximum mean discrepancy (MMD) measure-based hypothesis test. Next, we will show that our proposed test will outperform frequentist MMD-based methods by yielding a smaller false rejection and acceptance rate of the null. Finally, we will show that we can embed our proposed hypothesis testing procedure within a generative adversarial network (GAN) framework as an application of our method. Using our novel BNP hypothesis test, this new GAN approach can help to mitigate the lack of diversity in the generated samples and produce a more accurate inferential algorithm compared to traditional techniques.

**Keywords:** Dirichlet process, two-sample hypothesis tests, Bayesian evidence, generative models, computational methods.

## 1. Introduction

The generative adversarial network (GAN) (Goodfellow et al., 2014) is a machine learning technique used to generate realistic-looking artificial samples. The general architecture of GANs consists of two subnetworks—a generator,  $G_{\mathbf{w}}$ , and a discriminator,  $D_{\boldsymbol{\theta}}$  with parameters  $\mathbf{w}$  and  $\boldsymbol{\theta}$ , respectively. The GAN is trained until the generator can produce samples that can fool the discriminator into classifying the fake data as real data. The parameters of  $G_{\mathbf{w}}$  and  $D_{\boldsymbol{\theta}}$  are trained by optimizing the loss function:

$$\arg \min_{\mathbf{w}} \max_{\boldsymbol{\theta}} \mathcal{L}(G_{\mathbf{w}}, D_{\boldsymbol{\theta}}),$$

where  $\mathcal{L}(G_w, D_\theta) = E_{F_U}[\ln(D_\theta(X))] + E_{F_U}[\ln(1 - D_\theta(G_w(U)))]$ , in which  $F_U$  is the distribution of the noise vector  $U$ , and  $\ln(\cdot)$  denotes the natural logarithm.

Although GANs are effective for producing realistic samples, the process involves optimizing a difficult minimax problem that often suffers from mode collapse. The mode collapse phenomenon occurs when the generator learns only a few modes of the data distribution. Therefore, increasing the variety of produced samples is still a crucial issue that needs to be ameliorated. Arjovsky and Bottou (2017) mentioned that, in optimization problem for GANs, as  $D_\theta$  approaches a local optimum, then  $\mathcal{L}(G_w, D_\theta)$  becomes weak in distinguishing between real and fake data, there by leading the GAN to miss many modes. This fact is known as gradient vanishing. Partially, this is because the discriminator has a low capacity to detect the lack of sample diversity (Zhang, 2021). In fact, the training examples are very sparse and the sample space has high dimensionality, so weak discriminators can only find a few modes at best. Several procedures based on modifying the cost function and architecture of GANs have been developed in the literature (Donahue et al., 2016; Dumoulin et al., 2016) to deal with this issue. However, in these proposed procedures we can only empirically observe that we mitigate mode collapse, but there are no detailed explanations as to why these methods achieve superior experimental results (Lin et al., 2018).

Many frequentist GANs based on MMD can be found in the literature (Dziugaite et al., 2015; Briol et al., 2019; Li et al., 2015). However, BNP methods, while powerful, have comparatively not received much attention. Expert knowledge can be incorporated into the prior distributions in a diagnostic setting. This proves to be a hindrance for the statistician who wishes to be Bayesian with minimal assumptions. This paper seeks to fill this crucial gap. Specifically, we propose a semi-BNP counterpart of the two-sample MMD kernel-based test between data distribution  $F$  and  $F_{G_w}$  by placing the DP prior only on  $F$  not on  $F_{G_w}$  and extending it for machine learning tasks and training GANs. More precisely, our framework unifies concepts of the MMD measurement, the BNP inference, and the relative belief (RB) ratios to leverage their respective benefits into a single discriminator. Furthermore, we will embed our proposed discriminator within a GAN framework and investigate the ability of our discriminator to reduce mode collapse and increase the ability of the generator to fool the discriminator more effectively than the frequentist counterpart.

The paper is organized as follows: In Section 2 and 3 we discuss previous works and methods related to our work. We introduce our semi-BNP test in Section 4 and prove some theoretical properties of our proposed test. In Section 5, we apply our semi-BNP test as the discriminator in the GAN and run numerical experiments testing the novel semi-BNP GAN. Lastly, we conclude the paper in Section 7 and discuss some future directions of our proposed work.

## 2. Previous Work

Previous work has framed the discriminator of a GAN as a nonparametric two-sample hypothesis test. Here, the discriminator  $D$  is a two-sample test constructed based on a measure of discrepancy  $\delta$  to distinguish the fake data from the real data, and  $G_w$  is trained by optimizing a simpler objective function as

$$\arg \min_w \delta(F, F_{G_w}),$$

where  $F_{G_w}$  is the distribution of the generator. In fact,  $D$  attempts to continuously train  $G_w$  by checking the null hypothesis  $\mathcal{H}_0 : F = F_{G_w}$  until the difference between two distributions is indistinguishable. This technique leads to omitting the neural network from  $D$ , whose optimization may lead to a vanishing gradient. A commonly used discrepancy measure for  $\delta$  is the MMD, which is a kernel-based measure (Gretton et al., 2012). For given  $\mathbf{X}, \mathbf{X}' \stackrel{i.i.d.}{\sim} F, \mathbf{Y}, \mathbf{Y}' \stackrel{i.i.d.}{\sim} F_{G_w}$ , the MMD can be computed by

$$MMD^2(F, F_{G_w}) = E_F[k(\mathbf{X}, \mathbf{X}')] - 2E_{F, F_{G_w}}[k(\mathbf{X}, \mathbf{Y})] + E_{F_{G_w}}[k(\mathbf{Y}, \mathbf{Y}')], \quad (1)$$

via applying the kernel trick to compute the inner product between  $\mathbf{X}$  and  $\mathbf{Y}$  in an infinite feature space  $\mathcal{F}$  as  $k(\mathbf{X}, \mathbf{Y}) = \langle \mathbf{X}, \mathbf{Y} \rangle_{\mathcal{F}}$ . The MMD is 0 if and only if  $F = F_{G_w}$ , where  $\mathcal{F}$  corresponds to a universal reproducing kernel Hilbert space (RKHS). The Gaussian kernel, defined as  $k_{G_\sigma}(\mathbf{X}, \mathbf{Y}) = \exp(-\frac{\|\mathbf{X}-\mathbf{Y}\|^2}{2\sigma^2})$  with bandwidth parameter  $\sigma$ , is a common universal kernel used in MMD. In practice, distributions  $F$  and  $F_{G_w}$  are not accessible and then the biased, empirical estimator of (1) is calculated as

$$MMD_{n,m}^2(F, F_{G_w}) = \frac{1}{n^2} \sum_{i \neq j}^n k(\mathbf{X}_i, \mathbf{X}_j) - \frac{2}{mn} \sum_{i=1}^n \sum_{j=1}^m k(\mathbf{X}_i, \mathbf{Y}_j) + \frac{1}{m^2} \sum_{i \neq j}^m k(\mathbf{Y}_i, \mathbf{Y}_j), \quad (2)$$

where  $\mathbf{X}_1, \dots, \mathbf{X}_n$  is a real dataset and  $\mathbf{Y}_1, \dots, \mathbf{Y}_m$  is a sample generated from  $F_{G_w}$ .

Moreover, Li et al. (2015) considered  $k(\mathbf{X}, \mathbf{Y}) = \sum_{t=1}^T k_{G_{\sigma(t)}}(\mathbf{X}, \mathbf{Y})$  in (2) and then used it to train the generator. Independently of Li et al. (2015), Dziugaite et al. (2015) proposed the same method to train  $G_w$  but based on using a Bayesian optimization sequential design to set a value for  $\sigma$  and the number of neurons in each layer of network  $G_w$ . Li et al. (2017) proposed a learning technique by optimizing  $\arg \min_w \max_\phi MMD^2(F, F_{G_w})$  based on

considering  $k(\mathbf{X}, \mathbf{Y}) = \sum_{t=1}^T k_{G_{\sigma(t)}}(f_\phi(\mathbf{X}), f_\phi(\mathbf{Y}))$  for some injective parametrized functions  $f_\phi$  instead of setting a fixed Gaussian kernel. They argued this approach can be used to reduce the effect of the sample variance in training the generator. There are also a few works that consider some other discrepancy measures to train GANs such as the  $f$ -divergence measure (Nowozin et al., 2016), the Wasserstein distance (Arjovsky et al., 2017), and the total variation distance (Lin et al., 2018). However, the MMD is a kernel-based measure that can also be applied to data that are not in Euclidean space, which is useful for modeling complicated datasets such as images, where GANs are typically applied (Sejdinovic et al., 2013).

Previous work in applying MMD as a training criterion in GANs has only looked at the MMD as a test statistic in a frequentist two-sample test (Li et al., 2015; Dziugaite et al., 2015; Li et al., 2017; Bińkowski et al., 2018; Briol et al., 2019). However, these procedures are still liable to the drawbacks of frequentist testing. For instance, for a given permissible type I error rate (the probability of wrongly rejecting  $\mathcal{H}_0$  when it is true), denoted by  $\alpha$ ,  $\mathcal{H}_0$  is rejected if the values of Equation (2) greater than some threshold  $c_\alpha$ .

The corresponding  $p$ -value can also be computed by

$$2 \min\{P(MMD^2(F, F_{G_w}) > c_\alpha), MMD^2(F, F_{G_w}) < c_\alpha)\},$$

which leads the test to reject  $\mathcal{H}_0$  if it is less than  $\alpha$ . Li et al. (2017) mentioned that if (2) is not sufficiently larger than  $c_\alpha$  when  $\mathcal{H}_0$  is not true for some finite samples, the null

hypothesis  $\mathcal{H}_0$  is not rejected and then  $F_{G_w}$  cannot be distinguished from  $F$ . On the other hand, there is a relationship between  $\alpha$  and the probability of failing to reject the false null hypothesis (type II error), denoted by  $\beta$ , as  $\alpha + \beta \leq 1$ . The decrease in one of the errors causes an increase in the other one. Therefore we cannot arbitrarily drive to type I error rate to zero.

Moreover, the  $p$ -value in frequentist tests does not allow researchers to provide evidence for the null hypothesis while also exaggerating the evidence against the null hypothesis (Al-Labadi et al., 2022a). When  $\mathcal{H}_0$  should be rejected, the  $p$ -value in frequentist tests goes to zero as the sample size increases. Although it is known as a desirable feature of the  $p$ -value, a non-desirable feature is that the  $p$ -values are uniformly distributed between 0 and 1 under the null hypothesis. This distribution holds regardless of the sample size which means that increasing the sample size will not help to gain evidence for the null hypothesis in this case (Rouder et al., 2009).

Previous work has been developed to deal with these problems by proposing Bayesian counterparts to popular frequentist two-sample tests (Kelter, 2021; Al-Labadi and Zarepour, 2017; Al-Labadi, 2021; Al-Labadi et al., 2022a). In BNP hypothesis testing, we model the unknown distributions using infinite dimensional probability distributions as prior beliefs. One strategy to perform the BNP two-sample hypothesis test is to place a BNP prior on two unknown distributions being compared under the null and alternative hypothesis. Then the Bayes factor, which is the ratio of the marginal likelihood of data under the null to the alternative, is used to assess the null hypothesis. This strategy requires the calculation of the marginal likelihoods that are usually intractable to compute, so we must resort to costly approximate methods to conduct this test. The tests proposed by Holmes et al. (2015) and Borgwardt and Ghahramani (2009) are two examples of BNP tests that utilize marginal likelihood computation, and their practical usage in high-dimensional statistics is low due to this computational issue.

The construction of tests using the Bayes factor is based on placing a prior  $\pi(\cdot|\mathcal{H}_0)$  on  $\mathcal{H}_0$ , a prior  $\pi(\cdot|\mathcal{H}_1)$  on alternative hypothesis  $\mathcal{H}_1$  and a discrete mass of probability  $p(\mathcal{H}_0)$  for  $\mathcal{H}_0$ . In general, the elicitation of these three components is unclear, and practitioners often choose the quantities arbitrarily, leading to incorrect inference. Another concern of using Bayes factors is their calibration to indicate whether weak or strong evidence is attained. For example, Jeffreys (1961) and Kass and Raftery (1995) proposed similar rules to calibrate Bayes factors but García-Donato and Chen (2005) pointed out that such rules are inappropriate to calibrate Bayes factors as they ignore the randomness of the data and, again, lead to improper inference. In some Bayesian tests, the posterior distribution of a single hypothesis is only considered to judge the null as a posterior belief where there is no clear line between evidence for or against the null in this procedure. In addition, the posterior probability measures the belief that the null is true given the observed sample but does not present evidence. Hence, by considering a small prior belief for the null, the posterior belief will be obtained small even if  $\mathcal{H}_0$  is true, unless we have a large amount of data (Evans, 2015).

Another strategy is to compute a discrepancy measure between BNP posteriors of two unknown distributions  $F_1$  and  $F_2$ , denoted by  $\delta(F_1^{pos}, F_2^{pos})$  and compare it with the corresponding difference between BNP priors,  $\delta(F_1^{pri}, F_2^{pri})$  through the RB ratio (Al-Labadi et al., 2022a; Al-Labadi, 2021; Al-Labadi and Zarepour, 2017; Zhang et al., 2022). The con-

centration of  $\delta(F_1^{pos}, F_2^{pos})$  around zero being smaller than  $\delta(F_1^{pri}, F_2^{pri})$  indicates that the samples support the null hypothesis and vice versa. For instance, Al-Labadi et al. (2022a) proposed a BNP multi-sample test based on this strategy by placing the Dirichlet process (DP) prior on unknown distributions and using the energy distance as the discrepancy measure  $\delta$  with applications in high-dimensional data.

The DP is the most commonly used prior in BNP inference and can be viewed as an infinite-dimensional generalization of the Dirichlet distribution constructed around a fixed probability measure, whose variation is controlled by a positive real number. Although a particular case of the test of Al-Labadi et al. (2022a) can be used to compare distributions  $F_1$  and  $F_2$ , it cannot be considered a convenient discriminator in training GANs. In GANs, the objective is updating the parameter  $\mathbf{w}$  of the deterministic generative neural network  $G_{\mathbf{w}}$ . Therefore, treating  $F_{G_{\mathbf{w}}}$  as an unknown distribution on which we place a BNP prior is nonsensical. Moreover, the energy distance is a member of the larger class of MMD kernel-based measures (Sejdinovic et al., 2013). From here it is obvious that choosing among a larger class can lead to designing more sensitive discrepancy measures to detect differences.

Using the RB ratio as the hypothesis criteria circumvents many of the problems with other Bayesian criteria mentioned above. For instance, the RB ratio presents statistical evidence that measures the change in belief, whereas, the posterior probability of the null presents statistical belief. This is also useful for statistical practitioners to express quantitatively the amount of evidence for or against a hypothesis (a calibration of the evidence) that  $p$ -values and Bayes factors unintuitively do not do, in contrast to the RB ratio (Evans, 2015). Additionally, this strategy does not require computationally burdensome calculations like Monte Carlo Markov chain (MCMC) methods that were required in the first strategy to compute marginal likelihoods. A comprehensive study that explains why the RB ratio is a more appropriate measure of evidence than the Bayes factor can also be found in Al-Labadi et al. (2023).

### 3. Ingredients

#### 3.1 Dirichlet Process: A BNP prior

The DP, introduced by Ferguson (1973), is the most commonly used prior in Bayesian nonparametric inference. It can be viewed as an infinite-dimensional generalization of the Dirichlet distribution constructed around  $H$  (the base measure), a fixed probability measure, whose variation is controlled by  $a$  (the concentration parameter), a positive real number. To formally define the DP, consider a space  $\mathfrak{X}$  with a  $\sigma$ -algebra  $\mathcal{A}$  of subsets of  $\mathfrak{X}$ . For a base measure  $G$  on  $(\mathfrak{X}, \mathcal{A})$  and  $a > 0$ , a random probability measure  $F = \{F(A) : A \in \mathcal{A}\}$  is called a DP on  $(\mathfrak{X}, \mathcal{A})$ , denoted by  $F \sim DP(a, H)$ , if for every measurable partition  $A_1, \dots, A_k$  of  $\mathfrak{X}$  with  $k \geq 2$ , the joint distribution of the vector  $(F(A_1), \dots, F(A_k))$  has the Dirichlet distribution with parameters  $(aH(A_1), \dots, aH(A_k))$ . It is assumed that  $H(A_j) = 0$  implies  $F(A_j) = 0$  with probability one.

One of the most important properties of the DP is the conjugacy property—when the sample  $x = (x_1, \dots, x_n)$  is drawn from  $F \sim DP(a, H)$ , the posterior distribution of  $F$  given  $x$ , denoted by  $F^{pos}$ , is also a DP with concentration parameter  $a + n$  and base measure

$$H^* = a(a + n)^{-1}H + n(a + n)^{-1}F_n,$$

where  $F_n$  denotes the empirical cumulative distribution function of the sample  $x$ . Note that,  $H^*$  is a convex combination of the base measure  $H$  and  $F_n$ . Therefore,  $H^* \rightarrow H$  as  $a \rightarrow \infty$  while  $H^* \rightarrow F_n$  as  $a \rightarrow 0$ . On the other hand, when  $n \rightarrow \infty$ ,  $H^*$  converges to true cumulative distribution function which generates the data, by the Glivenko-Cantelli theorem. A guideline for choosing the hyperparameters  $a$  and  $H$  for the test of equality distributions will be covered in Section 3.

Bondesson (1982) and Sethuraman (1994) proposed two infinite series representations as alternative definitions for DP. The construction of Sethuraman (1994) is known as the stick-breaking representation and is a popularly used method in DP inference. However, Zarepour and Al-Labadi (2012) mentioned that, unlike the series of Bondesson (1982), the construction of the stick-breaking representation does not include any normalization terms to convert it to a probability measure. Zarepour and Al-Labadi (2012) also remarked that simulating from these infinite series is applicable only if a truncating approach is used for the terms inside the series. They suggested a truncation for the representation of Bondesson (1982) and referred to the upper bound proposed by Muliere and Tardella (1998) to approximate samples from stick-breaking representation.

In contrast, Ishwaran and Zarepour (2002) proposed the following representation to facilitate simulation of the DP. Let

$$F_N = \sum_{i=1}^N J_{i,N} \delta_{Y_i}, \quad (3)$$

where  $(J_{1,N}, \dots, J_{N,N}) \sim \text{Dirichlet}(a/N, \dots, a/N)$ . Ishwaran and Zarepour (2002) showed that  $(F_N)_{N \geq 1}$  converges in distribution to  $F$ , where  $F_N$  and  $F$  are random values in the space  $M_1(\mathbb{R})$  of probability measures on  $\mathbb{R}$  endowed with the topology of weak convergence. Thus, to generate  $(J_{i,N})_{1 \leq i \leq N}$  put  $J_{i,N} = H_{i,N} / \sum_{i=1}^N H_{i,N}$ , where  $(H_{i,N})_{1 \leq i \leq N}$  is a sequence of i.i.d. Gamma( $a/N, 1$ ) random variables independent of  $(Y_i)_{1 \leq i \leq N}$ . This form of approximation leads to some results in Section 4 and 5.

### 3.2 Relative Belief Ratio: A Bayesian Evidence

The RB ratio (Evans, 2015) is a form of Bayesian evidence in hypothesis testing problems and has shown excellent performance in many statistical hypothesis testing procedures (Al-Labadi et al., 2022a,b, 2021). The RB ratio is defined by the ratio of the posterior density to the prior density at a particular parameter of interest in the population distribution whose correctness is under investigation. Precisely, for a statistical model  $(\mathfrak{X}, \mathcal{F})$  with  $\mathcal{F} = \{f_\theta : \theta \in \Theta\}$ , let  $\pi$  be a prior on the parameter space  $\Theta$  and  $\pi(\theta | x)$  be the posterior distribution of  $\theta$  after observing the data  $x$ . Consider a parameter of interest,  $\psi = \Psi(\theta)$  such that  $\Psi$  satisfies regularity conditions so that the prior density  $\pi_\Psi$  and the posterior density  $\pi_\Psi(\cdot | x)$  of  $\psi$  exist with respect to some support measure on the range space for  $\Psi$ . When  $\pi_\Psi$  and  $\pi_\Psi(\cdot | x)$  are continuous at  $\psi$ , the RB ratio for a value  $\psi$  is given by

$$RB_\Psi(\psi | x) = \pi_\Psi(\psi | x) / \pi_\Psi(\psi).$$

Otherwise for a sequence  $N_\delta(\psi)$ , the neighborhoods of  $\psi$  that converge nicely to  $\psi$  as  $\delta \rightarrow 0$ , the RB ratio is defined by  $RB_\Psi(\psi | x) = \lim_{\delta \rightarrow 0} \Pi_\Psi(N_\delta(\psi) | x) / \Pi_\Psi(N_\delta(\psi))$ , where

$\Pi_\Psi$  and  $\Pi_\Psi(\cdot|x)$  are the marginal prior and the marginal posterior probability measures, respectively.

Note that  $RB_\Psi(\psi|x)$  measures the change in the belief of  $\psi$  being the true value *a priori* to *a posteriori*. Therefore, it is a measure of evidence. If  $RB_\Psi(\psi|x) > 1$ , then the probability of  $\psi$  being the true value from a priori to a posteriori is increased, consequently there is evidence based on the data that  $\psi$  is the true value. If  $RB_\Psi(\psi|x) < 1$ , then the probability of  $\psi$  being the true value from a priori to a posteriori is decreased. Accordingly, there is evidence against based on the data that  $\psi$  being the true value. For the case  $RB_\Psi(\psi|x) = 1$  there is no evidence in either direction. For the null hypothesis  $\mathcal{H}_0 : \Psi(\theta) = \psi_0$ , it is obvious  $RB_\Psi(\psi_0|x)$  measures the evidence in favor of or against  $\mathcal{H}_0$ .

The possibility of calibrating RB ratios is a desirable feature that makes it attractive in hypothesis testing problems. After computing the RB ratio, it is very critical to know whether the obtained value represents strong or weak evidence for or against  $\mathcal{H}_0$ . A typical calibration of  $RB_\Psi(\psi_0|x)$  is given by the *strength of evidence*

$$Str_\Psi(\psi|x) = \Pi_\Psi [RB_\Psi(\psi|x) \leq RB_\Psi(\psi_0|x) | x]. \quad (4)$$

The value in (4) indicates that the posterior probability that the true value of  $\psi$  has a RB ratio no greater than that of the hypothesized value  $\psi_0$ . When  $RB_\Psi(\psi_0|x) < 1$ , there is evidence against  $\psi_0$ , then a small value of (4) indicates strong evidence against  $\psi_0$  because the posterior probability of the true value having RB ratio bigger is large. On the other hand, a large value for (4) indicates weak evidence against  $\psi_0$ . Similarly, when  $RB_\Psi(\psi_0|x) > 1$ , there is evidence in favor of  $\psi_0$ , then a small value of (4) indicates weak evidence in favor of  $\psi_0$ , while a large value of (4) indicates strong evidence in favor of  $\psi_0$ .

### 3.3 Radial Basis Function Kernels Family

The construction of MMD-based tests is proposed based on considering a kernel function with feature space corresponding to a universal RKHS. The radial basis function (RBF) kernel is the most well-known kernel family satisfying the above situation. For two vectors  $\mathbf{X}, \mathbf{Y} \in \mathbb{R}^d$ , the RBF kernel is represented by

$$k(\mathbf{X}, \mathbf{Y}) = h(\|\mathbf{X} - \mathbf{Y}\|/\sigma),$$

where,  $h$  is a function from  $\mathbb{R}^+$  to  $\mathbb{R}^+$ , and  $\sigma$  is the bandwidth parameter that indicates the kernel size. There are many functions assigned to  $h$ , for example, the Gaussian, Laplacian, Matern, and rational quadratic kernels, represented by

$$h_1(x) = \exp^{-\frac{x^2}{2}}, h_2(x) = \exp^{-x}, h_3(x) = \left(1 + \frac{x^2}{2\alpha}\right)^{-\alpha}, h_4(x) = (1 + \sqrt{2\nu}x) \exp^{-\sqrt{2\nu}x},$$

respectively; where,  $\alpha$  in  $h_3$  is a positive-valued scale-mixture parameter. The  $\nu$  in  $h_4$  is a parameter that controls the smoothness of the kernel results, for instance,  $h_4$  is the Laplacian kernel when  $\nu = 0.5$ , while it is converging to the Gaussian kernel when  $\nu \rightarrow \infty$  (Zhao et al., 2022; Genton, 2001).

One of the simplest kernel functions above is the Gaussian kernel, which is mostly used in machine learning problems and only depends on bandwidth parameter  $\sigma$ . The Gaussian

kernel tends to 0 and 1 when  $\sigma \rightarrow 0$  and  $\sigma \rightarrow \infty$ , respectively. Both situations lead to  $MMD^2$  in (1) being zero. Hence, the choice of the parameter  $\sigma$  has a crucial effect on the performance of this kernel. Numerous methods are proposed to choose the value of  $\sigma$ , however, there is no definitive optimization method for this problem. The median heuristic is one of the first methods used in choosing  $\sigma$  empirically. More precisely, for two samples  $\{\mathbf{X}_i\}_{i=1}^n$  and  $\{\mathbf{Y}_j\}_{j=1}^m$ , the  $\sigma$  is considered as the median of  $\{\|\mathbf{X}_i - \mathbf{Y}_j\|^2 : 1 \leq i \leq n, 1 \leq j \leq m\}$ , which is mostly used in kernel-based tests (Schölkopf et al., 2002). Selecting  $\sigma$  based on maximizing the power of such tests is another strategy considered by Jitkrittum et al. (2017). Regarding the choice of  $\sigma$  in kernel-based GANs, a common idea is assigning several fixed values to  $\sigma$  and then considering the mixture of their corresponding Gaussian kernel. This strategy has received much attention and shown an acceptable performance in training GANs. For further details, see Li et al. (2015) and Li et al. (2017).

### 3.4 Training Evaluation

Evaluating the quality of samples generated by GANs is considered to assess the mode collapse problem (Zhang, 2021). The inception score, proposed by Salimans et al. (2016), is one common tool used evaluate GANs. Let  $\mathbf{Y}$  represent a sample generated by the generator  $G_{\mathbf{w}}$  and  $z$  be the label given to  $\mathbf{Y}$  by the discriminator. For instance, if  $\mathbf{Y}$  can not be distinguished from the real dataset,  $z = 1$ ; otherwise,  $z = 0$ . Then, the inception score is given by

$$\begin{aligned} IS &= \exp \left\{ E_{\mathbf{Y}} \left[ D_{KL}(p(z|\mathbf{Y}), E_{\mathbf{Y}}[p(z|\mathbf{Y})]) \right] \right\} \\ &= \exp \left\{ H(E_{\mathbf{Y}}[p(z|\mathbf{Y})]) - E_{\mathbf{Y}}(H(p(z|\mathbf{Y}))) \right\} \end{aligned}$$

where  $p(z|Y)$  is the probability that  $\mathbf{Y}$  takes label  $z$  by the discriminator,  $D_{KL}(\cdot, \cdot)$  denotes the Kullback-Leibler divergence, and  $H(\cdot)$  denotes the entropy. Higher values of  $IS$  indicate greater sample diversity. The lowest value of  $IS$  is achieved if and only if for any  $\mathbf{Y}$  generated by  $G_{\mathbf{w}}$ ,  $p(z|Y) = E_Y[p(z|Y)]$ . It means the probability that the discriminator gives label  $z$  to  $\mathbf{Y}$  is the same, for any  $\mathbf{Y}$  generated by the generator.

If a generated sample with low quality, the entropy of  $E_Y[p(z|Y)]$  and  $p(z|Y)$  can still be, respectively, high and low, which leads to a good inception score. Che et al. (2016) also mentioned this issue and proposed the mode score function to deal with this issue by

$$MS = \exp \left\{ E_{\mathbf{Y}} \left[ D_{KL}(p(z|\mathbf{Y}), p(z)) \right] - D_{KL}(E_{\mathbf{Y}}[p(z|\mathbf{Y})], p(z)) \right\}, \quad (5)$$

where  $p(z)$  is the distribution of labels in the training data. The first part of (5) assesses the quality of the generated sample and the last part deals to assess the variety of the generated sample. The higher values of  $MS$  again indicate greater diversity and higher quality for the generated sample. However, Che et al. (2016) pointed out that the above score does not work well when training datasets are unlabeled.

Despite using Kullback-Leibler divergence, Zhang (2021) designed a matching score to evaluate the sample qualification as follows. For a real dataset  $U = \{\mathbf{X}_1, \dots, \mathbf{X}_n\}$ , let  $\mathbf{w}^*$  be a parameter of  $G_{\mathbf{w}}$  that optimized the desired GAN objective function. Then, for any similarity function  $s(\cdot, \cdot)$ , the matching score between the real and generated sample is given



by

$$MCS = \frac{1}{n} \max_{t \in \mathcal{T}} \sum_{i=1}^n s(\mathbf{X}_i, \mathbf{Y}_{t(i)}(\mathbf{w}^*)), \quad (6)$$

where  $\mathcal{T}$  is all permutations of  $n$  elements in  $\{1, \dots, n\}$  and  $V = \{\mathbf{Y}_{t(1)}(\mathbf{w}^*), \dots, \mathbf{Y}_{t(n)}(\mathbf{w}^*)\}$  drawn from the trained generator  $G_{\mathbf{w}^*}$ . A larger matching score guarantees more modes in the generated manifold. Since the computation of  $n!$  terms in (6) is time-consuming, Zhang (2021) applied the maximum bipartite matching (MBM) algorithm to find the optimal permutation of realistic samples to the corresponding permutation of the real dataset and then uses the cosine similarity,

$$s(\mathbf{X}_i, \mathbf{Y}_{t(i)}(\mathbf{w}^*)) = \frac{\sum_{j=1}^d (\mathbf{X}_{ij} \mathbf{Y}_{t(i)j}(\mathbf{w}^*))}{\sqrt{\sum_{j=1}^d \mathbf{X}_{ij} \sum_{j=1}^d \mathbf{Y}_{t(i)j}(\mathbf{w}^*)}},$$

where  $\mathbf{Y}_{t(i)} \in \mathbb{R}^d$  and  $\mathbf{Y}_{t(i)j}$  denotes the  $j$ -th element of the vector  $\mathbf{Y}_{t(i)}$ . The Ford–Fulkerson (FF), Edmonds–Karp (EK), and Hopcroft–Karp (HK) are among the most famous matching algorithms to compute this permutation (Ford and Fulkerson, 1956; Edmonds and Karp, 1972; Hopcroft and Karp, 1973). A particular consideration that should be taken into account is the running time of these algorithms. For example, the running time of the FF, EK, and HK algorithms are  $O(|U \cup V|f)$ ,  $O(|U \cup V||E|^2)$ , and  $O(\sqrt{|U \cup V||E|})$ , respectively, where  $f$  is the maximum flow in the graph, and  $|\cdot|$  denotes the number of components in the relevant set.

#### 4. Constructing a Semi-BNP Two-sample Kernel-based Test Using RB Inferences

In this section, we introduce our novel Semi-BNP counterpart of the MMD distance to propose a two-sample test. Precisely, for two distributions  $F_1$  and  $F_2$ , the object of interest is to evaluate the hypothesis  $\mathcal{H}_0 : F_1 = F_2$ . Let  $F_1$  be a completely unknown distribution and  $F_2$  be any distribution with a complex generating process. For a given sample  $\mathbf{Y}_1, \dots, \mathbf{Y}_m$  from  $F_2$  and by assuming  $F_1^{pri} := F_1 \sim DP(a, H)$  for a non-negative value  $a$  and a fixed probability measure  $H$ , we propose the two-sample prior-based MMD as

$$\begin{aligned} MMD_{BNP}^2(F_1^{pri}, F_2) &= \sum_{\ell, t=1}^N J_{\ell, N} J_{t, N} k(\mathbf{V}_\ell, \mathbf{V}_t) - \frac{2}{m} \sum_{\ell=1}^N \sum_{t=1}^m J_{\ell, N} k(\mathbf{V}_\ell, \mathbf{Y}_t) \\ &+ \frac{1}{m^2} \sum_{\ell, t=1}^m k(\mathbf{Y}_\ell, \mathbf{Y}_t), \end{aligned} \quad (7)$$

where,  $(J_{1, N}, \dots, J_{N, N})$  is sampled from Dirichlet( $a/N, \dots, a/N$ ),  $\mathbf{V}_1, \dots, \mathbf{V}_N \stackrel{i.i.d.}{\sim} H$ , and  $N$  is the number of terms in the DP approximation  $\sum_{\ell=1}^N J_{\ell, N} \delta_{\mathbf{V}_\ell}$  proposed by Ishwaran and Zarepour (2002). We are proposing this method for the purpose of considering a discriminator of GANs as a two-sample test in training the generative neural network. As we will explain in more detail in the next section, the proposed discriminator will be used to

compare the distribution of the real data with the deterministic generator's synthetic data to update the generator's parameter. Since the push forward measure of the generator is parameterized by the deep neural network parameter, we only impose the DP prior on the distribution of the real data which leads us to our proposed Semi-BNP approach.

**Theorem 1** *For a non-negative real value  $a$  and fixed probability distribution  $H$ , let  $F_1^{pri} := F_1 \sim DP(a, H)$  and  $k(\cdot, \cdot)$  be any kernel with feature space corresponding to a universal RKHS. Then,*

- i.  $E_{F_1^{pri}}(MMD_{BNP}^2(F_1^{pri}, F_2)) \rightarrow MMD_{N,m}^2(H, F_2)$ , as  $a \rightarrow \infty$ ,*
- ii.  $E_{F_1^{pri}}(MMD_{BNP}^2(F_1^{pri}, F_2))$  converges in probability at rate  $O((N+m)^{-1/2})$  to  $MMD^2(H, F_2)$  as  $a \rightarrow \infty$ , if  $k(\mathbf{z}, \mathbf{z}') < K$ , for any  $\mathbf{z}, \mathbf{z}' \in \mathbb{R}^d$ ,*
- iii.  $E(MMD_{BNP}^2(F_1^{pri}, F_2)) \rightarrow MMD^2(H, F_2)$  as  $a \rightarrow \infty$ ,  $N \rightarrow \infty$ , and  $m \rightarrow \infty$ .*

**Proof** Since  $(J_{1,N}, \dots, J_{N,N}) \sim \text{Dirichlet}(\frac{a}{N}, \dots, \frac{a}{N})$ ,  $E_{F_1^{pri}}(J_{\ell,N}) = \frac{1}{N}$  and  $E_{F_1^{pri}}(J_{\ell,N}J_{t,N}) = \frac{a}{(a+1)N^2}$ . Applying these properties in (7) results in

$$\begin{aligned} E_{F_1^{pri}}(MMD_{BNP}^2(F_1^{pri}, F_2)) &= \frac{a}{(a+1)N^2} \sum_{\ell,t=1}^N k(\mathbf{V}_\ell, \mathbf{V}_t) - \frac{2}{Nm} \sum_{\ell=1}^N \sum_{t=1}^m k(\mathbf{V}_\ell, \mathbf{Y}_t) \\ &\quad + \frac{1}{m^2} \sum_{\ell,t=1}^m k(\mathbf{Y}_\ell, \mathbf{Y}_t), \end{aligned}$$

and letting  $\alpha \rightarrow \infty$  completes the proof of (i). To prove (ii), let

$$\begin{aligned} \Delta &= \lim_{a \rightarrow \infty} E_{F_1^{pri}}(MMD_{BNP}^2(F_1^{pri}, F_2)) - MMD^2(H, F_2), \\ \Delta' &= MMD_{N,m}^2(H, F_2) - MMD^2(H, F_2). \end{aligned}$$

Following Gretton et al. (2012, Theorem 7) and then applying part (i), gives us

$$\begin{aligned} \Pr \left\{ |\Delta| > \frac{2\sqrt{K}(\sqrt{N} + \sqrt{m})}{\sqrt{Nm}} + \epsilon \right\} &= \Pr \left\{ |\Delta'| > \frac{2\sqrt{K}(\sqrt{N} + \sqrt{m})}{\sqrt{Nm}} + \epsilon \right\} \\ &\leq 2 \exp \frac{-\epsilon^2 Nm}{2K(N+m)}, \end{aligned} \quad (8)$$

for any  $\epsilon > 0$ , which concludes the results. To prove (iii), it is sufficient to compute the following conditional expectation,

$$E(MMD_{BNP}^2(F_1^{pri}, F_2)) = E_{H, F_2}(E_{F_1^{pri}}(MMD_{BNP}^2(F_1^{pri}, F_2))). \quad (9)$$

Since  $k(\cdot, \cdot)$  corresponds to a universal RKHS and sets  $\{V_i\}_{i=1}^N$  and  $\{Y_i\}_{i=1}^m$  include identically distributed random variables, separately, we have from the proof of (i):

$$(9) = \frac{a(N-1)}{(a+1)N} E_H[k(\mathbf{V}_1, \mathbf{V}_2)] - 2E_{H, F_2}[k(\mathbf{V}_1, \mathbf{Y}_1)] + \frac{m-1}{m} E_{F_2}[k(\mathbf{Y}_1, \mathbf{Y}_2)]. \quad (10)$$

The proof is concluded by letting  $a \rightarrow \infty$ ,  $N \rightarrow \infty$ , and  $m \rightarrow \infty$  in the above equation. ■

The next result plays a crucial role in choosing  $H$  in the proposed test.

**Corollary 2** *Under assumptions of Theorem 1, we have*

- i.  $E(MMD_{BNP}^2(F_1^{pri}, F_2)) \leq MMD^2(H, F_2)$ , for any  $N, m \in \mathbb{N}$  and  $a \in \mathbb{R}^+$ , where  $\mathbb{N}$  denotes the natural numbers and  $\mathbb{R}^+$  denotes the positive real numbers,
- ii.  $E(MMD_{BNP}^2(F_1^{pri}, F_2)) \rightarrow 0$  as  $a \rightarrow \infty$ ,  $N \rightarrow \infty$ , and  $m \rightarrow \infty$ , if and only if  $H = F_2$ .

**Proof** Consider Equation (10) in the proof of Theorem 1. Since  $\frac{m-1}{m} < 1$  and  $\frac{a(N-1)}{(a+1)N} < 1$ , then, for any  $N, m \in \mathbb{N}$  and  $a \in \mathbb{R}^+$ ,

$$(10) < E_H[k(\mathbf{V}_1, \mathbf{V}_2)] - 2E_{H, F_2}[k(\mathbf{V}_1, \mathbf{Y}_1)] + E_{F_2}[k(\mathbf{Y}_1, \mathbf{Y}_2)],$$

which concludes the proof of (i). The proof of (ii) is immediately concluded by the definition of the MMD measure given by (1); hence, it is omitted. ■

The previous statements present some asymptotic properties for the expectation of the prior-based MMD measure. The stochastic boundedness property of  $MMD_{BNP}^2(F_1^{pri}, F_2)$  will be discussed in the next theorem.

**Theorem 3** *For a non-negative real value  $a$  and fixed probability distribution  $H$ , let  $F_1^{pri} := F_1 \sim DP(a, H)$ , and  $k(\cdot, \cdot)$  be any kernel function with feature space corresponding to a universal RKHS. Assume that  $k(\mathbf{z}, \mathbf{z}') < K$ , for any  $\mathbf{z}, \mathbf{z}' \in \mathbb{R}^d$ . Then,  $MMD_{BNP}^2(F_1^{pri}, F_2)$  converges in probability at rate  $O((N + m)^{-1/2})$  to  $MMD^2(H, F_2)$  as  $a \rightarrow \infty$ .*

**Proof** For samples  $\{\mathbf{V}_\ell\}_{\ell=1}^N$  and  $\{\mathbf{Y}_\ell\}_{\ell=1}^m$ , respectively, from  $H$  and  $F_2$ , the triangle inequality implies

$$\begin{aligned} \left| MMD_{BNP}^2(F_1^{pri}, F_2) - MMD_{N,m}^2(H, F_2) \right| &\leq \sum_{\ell, t=1}^N \left| J_{\ell, N} J_{t, N} - \frac{1}{N^2} \right| k(V_\ell, V_t) \\ &\quad + \frac{2}{m} \sum_{\ell}^N \sum_{t=1}^m \left| J_{\ell, N} - \frac{1}{N} \right| k(V_\ell, Y_t). \end{aligned}$$

By Proposition 7 presented by Appendix A, which provides some theoretical properties of the DP approximation given in (3), the right-hand side of the above inequality converges almost surely to 0 as  $a \rightarrow \infty$  for fixed  $N$ . It implies

$$MMD_{BNP}^2(F_1^{pri}, F_2) \xrightarrow{a.s.} MMD_{N,m}^2(H, F_2). \quad (11)$$

To prove part (ii) of Theorem 1, we see that  $MMD_{N,m}^2(H, F_2)$  converges in probability at rate  $O((N + m)^{-1/2})$  to  $MMD^2(H, F_2)$  according to Gretton et al. (2012, Theorem 7) and a similar argument used in (8). Hence, the proof is completed. ■

After observing samples  $\mathbf{X}_1, \dots, \mathbf{X}_n$  from  $F_1$  and considering  $\mathbf{V}_1^*, \dots, \mathbf{V}_N^* \stackrel{i.i.d.}{\sim} H^*$ , and  $(J_{1,N}^*, \dots, J_{N,N}^*) \sim Dir(\frac{a+n}{N}, \dots, \frac{a+n}{N})$ , we update the prior-based MMD (7) to the posterior one as

$$\begin{aligned} MMD_{BNP}^2(F_1^{pos}, F_2) &= \sum_{\ell, t=1}^N J_{\ell, N}^* J_{t, N}^* k(\mathbf{V}_\ell^*, \mathbf{V}_t^*) - \frac{2}{m} \sum_{\ell=1}^N \sum_{t=1}^m J_{\ell, N}^* k(\mathbf{V}_\ell^*, \mathbf{Y}_t) \\ &\quad + \frac{1}{m^2} \sum_{\ell, t=1}^m k(\mathbf{Y}_\ell, \mathbf{Y}_t), \end{aligned} \quad (12)$$

where,  $H^* = a/(a+n)H + n/(a+n)F_{n1}$ ,  $F_{n1}$  denotes the empirical distribution of observed data, and  $F_1^{pos}$  refers to  $F_1 | \mathbf{X}_1, \dots, \mathbf{X}_n \sim DP(a+n, H^*)$ . The following Theorem presents asymptotic properties of  $MMD_{BNP}^2(F_1^{pos}, F_2)$ .

**Theorem 4** *For a non-negative real value  $a$  and fixed probability distribution  $H$ , let  $F_1^{pri} := F_1 \sim DP(a, H)$  and  $k(\cdot, \cdot)$  be any continuous kernel function with feature space corresponding to a universal RKHS. Assume that  $k(\mathbf{z}, \mathbf{z}') < K$ , for any  $\mathbf{z}, \mathbf{z}' \in \mathbb{R}^d$ . Then, for a given sample  $\mathbf{X}_1, \dots, \mathbf{X}_n$  from distribution  $F_1$ ,*

- i.  $E(MMD_{BNP}^2(F_1^{pos}, F_2)) \rightarrow MMD^2(H, F_2)$ , as  $a \rightarrow \infty$ ,  $N \rightarrow \infty$ , and  $m \rightarrow \infty$ ,*
- ii.  $MMD_{BNP}^2(F_1^{pos}, F_2)$  converges in probability at rates  $O((N+m)^{-1/2})$  to  $MMD^2(H, F_2)$ , as  $a \rightarrow \infty$ ,*
- iii.  $E(MMD_{BNP}^2(F_1^{pos}, F_2)) \rightarrow MMD^2(F_1, F_2)$ , as  $N \rightarrow \infty$ ,  $n \rightarrow \infty$ , and  $m \rightarrow \infty$ ,*
- iv.  $MMD_{BNP}^2(F_1^{pos}, F_2)$  converges in probability at rates  $O((N+m)^{-1/2})$  to  $MMD^2(F_1, F_2)$ , as  $n \rightarrow \infty$ .*

**Proof** Since the DP is a conjugate prior, it follows from the proof of Theorem 1:

$$\begin{aligned} E(MMD_{BNP}^2(F_1^{pos}, F_2)) &= h(a, n, N) E_{H^*}[k(\mathbf{V}_1^*, \mathbf{V}_2^*)] - 2E_{H^*, F_2}[k(\mathbf{V}_1^*, \mathbf{Y}_1)] \\ &\quad + \frac{m-1}{m} E_{F_2}[k(\mathbf{Y}_1, \mathbf{Y}_2)], \end{aligned} \quad (13)$$

where  $h(a, n, N) = \frac{(a+n)(N-1)}{(a+n+1)N}$ . On the other hand, since  $H^* \rightarrow H$  as  $a \rightarrow \infty$ , the chance of sampling from  $H$  and  $F_{n1}$  tends, respectively, to one and zero, which implies  $V_i^* \rightarrow V_i$ , where  $V_i \sim H$ , for  $i = 1, 2$ . Applying the continuous mapping theorem implies  $k(\mathbf{V}_1^*, \mathbf{V}_2^*) \rightarrow k(\mathbf{V}_1, \mathbf{V}_2)$  and  $k(\mathbf{V}_1^*, \mathbf{Y}_1) \rightarrow k(\mathbf{V}_1, \mathbf{Y}_1)$ . Since  $k(\cdot, \cdot)$  is bounded above by  $K$ , the dominated convergence theorem implies  $E_{H^*}[k(\mathbf{V}_1^*, \mathbf{V}_2^*)] \rightarrow E_H[k(\mathbf{V}_1, \mathbf{V}_2)]$  and  $E_{H^*, F_2}[k(\mathbf{V}_1^*, \mathbf{Y}_1)] \rightarrow E_{H, F_2}[k(\mathbf{V}_1, \mathbf{Y}_1)]$ . Since  $h(a, n, N) \rightarrow 1$  as  $a \rightarrow \infty$ ,  $N \rightarrow \infty$  and  $m/(m-1) \rightarrow 1$ , as  $m \rightarrow \infty$ , the proof of (i) is concluded. For (ii), considering the conjugacy property of the DP for equation (11) in the proof of Theorem 3 implies  $MMD_{BNP}^2(F_1^{pos}, F_2)$  converges almost surely to  $MMD_{N, m}^2(H^*, F_2)$ , as  $a \rightarrow \infty$ .

Also, the convergence of  $\mathbf{V}_i^*$ 's to  $\mathbf{V}_i$ 's, as  $a \rightarrow \infty$ , implies  $MMD_{BNP}^2(F_1^{pos}, F_2) \xrightarrow{a.s.} MMD_{N, m}^2(H, F_2)$ . The final results follow with a similar argument in the proof of Theorem 3. To prove (iii) and (iv),  $F_{n1} \rightarrow F_1$ , and then  $H^* \rightarrow F_1$  as  $n \rightarrow \infty$  by the Glivenko-Cantelli theorem. It indicates that the probability of sampling from  $H$  and  $F_{n1}$  tends, respectively, to zero and one. Therefore,  $V_i^* \rightarrow X_i$  as  $n \rightarrow \infty$ , where  $X_i \sim F_1$ , for  $i = 1, 2$ . The proof of (iii) is completed with the same strategy as the proof of (i) by letting  $N \rightarrow \infty$ ,  $n \rightarrow \infty$ ,

and  $m \rightarrow \infty$  in (13). The proof of (iv) is also concluded with a similar argument that in (ii), when  $n \rightarrow \infty$ .  $\blacksquare$

The next corollary presents the consistency property of the posterior-based MMD measure.

**Corollary 5** *Under the assumption of Theorem 4, then*

- i.  $E(MMD_{BNP}^2(F_1^{pos}, F_2)) \rightarrow 0$  if and only if  $H = F_2$ , as  $N \rightarrow \infty$ ,  $a \rightarrow \infty$ , and  $m \rightarrow \infty$ ,*
- ii.  $E(MMD_{BNP}^2(F_1^{pos}, F_2)) \rightarrow 0$  if and only if  $F_1 = F_2$ , as  $N \rightarrow \infty$ ,  $n \rightarrow \infty$ , and  $m \rightarrow \infty$ .*

**Proof** The proof is immediately followed by Theorem 4.  $\blacksquare$

We now present our semi-BNP test, where we propose to test the hypothesis:

$$\mathcal{H}_0 : MMD^2(F_1, F_2) = 0, \quad (14)$$

using the RB ratio. We link this problem to the RB inferences by considering  $\Psi = MMD^2(F_1, F_2)$  and  $\psi_0 = 0$  in Section 3.2. For such  $\psi_0$ , the RB ratio can be expressed by

$$RB_{MMD^2(F_1, F_2)}(0 | \mathbf{X}_1, \dots, \mathbf{X}_n) = \frac{\pi_{MMD^2(F_1, F_2)}(0 | \mathbf{X}_1, \dots, \mathbf{X}_n)}{\pi_{MMD^2(F_1, F_2)}(0)}, \quad (15)$$

where,  $\pi_{MMD^2(F_1, F_2)}(\cdot | \mathbf{X}_1, \dots, \mathbf{X}_n)^1$  denotes density functions of  $MMD_{BNP}^2(F_1^{pos}, F_2)$  and  $\pi_{MMD^2(F_1, F_2)}(\cdot)$  denotes density functions of  $MMD_{BNP}^2(F_1^{pri}, F_2)$ .

The density in the denominator of (15) must support the null in order to reflect how well the data can support the null hypothesis based on the comparison between the prior and the posterior, utilizing the fundamental concepts of the RB ratio from Section 3.2. Here, supporting  $\mathcal{H}_0$  by  $\pi_{MMD^2}(\cdot)$  means that the prior density is centered around zero. To enforce this term on  $\pi_{MMD^2}(\cdot)$ , it is enough to set  $H = F_2$  in  $DP(a, H)$ , which is deduced from the Corollary 2, part (iii).

With regards to choosing the concentration parameter  $a$  in our proposed approach, we note that  $a$  controls the variation of  $F^{pri}$  around  $H$ , which controls the strength of belief that  $\mathcal{H}_0$  is true. On the other hand, it is recommended to choose  $a < n/2$  based on the definition of  $H^*$  in  $F^{pos}$  (Al-Labadi and Zarepour, 2017). The idea behind using such a value of  $a$  is to avoid the excessive effect of the prior  $H$  on the test results by considering the chance of sampling from the observed data at least twice the chance of generating samples from  $H$ . However, some computational methods in the literature are proposed to elicit  $a$  that one may be interested in using (Al-Labadi et al., 2022b; Al-Labadi, 2021). Both expectations of  $MMD_{BNP}^2(F_1^{pos}, F_2)$  and  $MMD_{BNP}^2(F_1^{pri}, F_2)$  tend to 0 as  $a \rightarrow \infty$ ,  $N \rightarrow \infty$ , and  $m \rightarrow \infty$ , respectively, according to Corollaries 2 and 5. Hence, both prior and posterior densities in (15) should be centered and coincided around 0. It causes the value of (15) becomes very close to 1 based on which no decision can be made about  $\mathcal{H}_0$ .

In this paper, we will empirically choose  $a$  to be less than  $n/2$  and then compute (15). For fixed  $a$ , Corollary 5 implies that  $MMD_{BNP}^2(F_1^{pos}, F_2)$  should be more dense

---

1. Note that the subscript  $(F_1, F_2)$  may be omitted whenever it is clear in the context.

than  $MMD_{BNP}^2(F_1^{pri}, F_2)$  at 0 if and only if  $\mathcal{H}_0$  is true. Hence, the value of (15) presents evidence for or against  $\mathcal{H}_0$ , if  $RB_{MMD^2}(0|\mathbf{X}_1, \dots, \mathbf{X}_n) > 1$  or  $RB_{MMD^2}(0|\mathbf{X}_1, \dots, \mathbf{X}_n) < 1$ , respectively. Following Section 3.2, the calibration of (15) is defined as:

$$\begin{aligned} Str_{MMD^2}(0|\mathbf{X}_1, \dots, \mathbf{X}_n) &= \Pi_{MMD^2}(RB_{MMD^2}(mmd^2|\mathbf{X}_1, \dots, \mathbf{X}_n) \\ &\leq RB_{MMD^2}(0|\mathbf{X}_1, \dots, \mathbf{X}_n)|\mathbf{X}_1, \dots, \mathbf{X}_n), \end{aligned} \quad (16)$$

where,  $\Pi_{MMD^2}(\cdot|\mathbf{X}_1, \dots, \mathbf{X}_n)$  is the cumulative distribution function corresponding to the density  $\pi_{MMD^2}(\cdot|\mathbf{X}_1, \dots, \mathbf{X}_n)$ . Particular attention should be paid here to the computation of (15) and (16). The densities used in (15) do not have explicit forms. Thus, we use their corresponding ecdf based on  $\ell$  sample sizes to estimate (15) and (16), respectively, as

$$\widehat{RB}_{MMD^2}(0|\mathbf{X}_1, \dots, \mathbf{X}_n) = \frac{\hat{\Pi}_{MMD^2}(\hat{d}_{i_0/M}|\mathbf{X}_1, \dots, \mathbf{X}_n)}{\hat{\Pi}_{MMD^2}(\hat{d}_{i_0/M})}, \quad (17)$$

$$\begin{aligned} \widehat{Str}_{MMD^2}(0|\mathbf{X}_1, \dots, \mathbf{X}_n) &= \sum_D (\hat{\Pi}_{MMD^2}(\hat{d}_{(i+1)/M}|\mathbf{X}_1, \dots, \mathbf{X}_n) \\ &\quad - \hat{\Pi}_{MMD^2}(\hat{d}_{i/M}|\mathbf{X}_1, \dots, \mathbf{X}_n)), \end{aligned} \quad (18)$$

where,

$$D = \left\{ 0 \leq i \leq M-1 : \widehat{RB}_{MMD^2}(\hat{d}_{i/W}|\mathbf{X}_1, \dots, \mathbf{X}_n) \leq \widehat{RB}_{MMD^2}(0|\mathbf{X}_1, \dots, \mathbf{X}_n) \right\},$$

in which  $M$  is a positive number,  $\hat{d}_{i/M}$  be the estimate of  $d_{i/M}$ , the  $(i/M)$ -th prior quantile of  $MMD_{BNP}^2(F_1^{pri}, F_2)$ ,

$$\widehat{RB}_{MMD^2}(\hat{d}_{i/M}|\mathbf{X}_1, \dots, \mathbf{X}_n) = \frac{\hat{\Pi}_{MMD^2}(\hat{d}_{\frac{i+1}{M}}|\mathbf{X}_1, \dots, \mathbf{X}_n) - \hat{\Pi}_{MMD^2}(\hat{d}_{\frac{i}{M}}|\mathbf{X}_1, \dots, \mathbf{X}_n)}{\hat{\Pi}_{MMD^2}(\hat{d}_{\frac{i+1}{M}}) - \hat{\Pi}_{MMD^2}(\hat{d}_{\frac{i}{M}})}$$

and  $i_0$  in (17) is chosen so that  $i_0/M$  is not too small (typically  $i_0/M = 0.05$ ). Further details are available in Algorithm 1. For fixed  $M$ , as  $N \rightarrow \infty$  and  $\ell \rightarrow \infty$ , then  $\hat{d}_{i/W}$  converges almost surely to  $d_{i/W}$  and (17) and (18) converge almost surely to (15) and (16), respectively. The following result due to Al-Labadi and Evans (2018, Proposition 6) gives the consistency of the proposed test. In the sense that, if  $\mathcal{H}_0$  is true, then (15) and (16) converges, respectively, almost surely to  $M/i_0 (> 1)$  and 1, as  $n \rightarrow \infty$ ; otherwise, both converge to 0.

---

**Algorithm 1** Pseudocode of semi-BNP two-sample MMD kernel test

---

- 1: Initialize  $a$ ,  $N$ ,  $\ell$ , and  $M$ .
- 2:  $H \leftarrow F_2$   
STEP 1: Computing the BNP MMD
- 3: **for**  $r \leftarrow 0$  to  $\ell$  **do**
- 4:   Generate an approximate sample of  $F_1 \sim DP(a, H)$  by using  $\sum_{i=1}^N J_{i,N} \delta_{\mathbf{v}_i}$ , where  $\{J_{i,N}\}_{i=1}^N \sim \text{Dirichlet}(\frac{a}{N}, \dots, \frac{a}{N})$ , and  $\{\mathbf{v}_i\}_{i=1}^N \sim H$ .
- 5:   Generate an approximate sample of  $F_1|\mathbf{x} \sim DP(a+n, H^*)$  by using  $\sum_{i=1}^N J_{i,N}^* \delta_{\mathbf{v}_i^*}$ , where  $\{J_{i,N}^*\}_{i=1}^N \sim \text{Dirichlet}(\frac{a+n}{N}, \dots, \frac{a+n}{N})$ , and  $\{\mathbf{v}_i^*\}_{i=1}^N \sim H^*$ .
- 6:   Use (7) and (12) for the samples generated in steps 4 and 5 to compute

$MMD_{BNP}^2(F_1^{pri}, F_2)$  and  $MMD_{BNP}^2(F_1^{pos}, F_2)$ , respectively.  
7: **end for**  
8: **return**  $\{MMD_{BNP_r}^2(F_1^{pri}, F_2)\}_{r=1}^\ell$  and  $\{MMD_{BNP_r}^2(F_1^{pos}, F_2)\}_{r=1}^\ell$   
**STEP 2: Estimating RB and Str**  
9:  $\widehat{\Pi}_{MMD^2}(\cdot|\mathbf{x}, \mathbf{y}) \leftarrow Ecdf(\{MMD_{BNP_r}^2(F_1^{pos}, F_2)\}_{r=1}^\ell)$   $\triangleright$  The ecdf of posterior-based MMD  
10:  $\widehat{\Pi}_{MMD^2}(\cdot) \leftarrow Ecdf(\{MMD_{BNP_r}^2(F_1^{pri}, F_2)\}_{r=1}^\ell)$   $\triangleright$  The ecdf of prior-based MMD  
11:  $\widehat{RB}_{MMD^2}(0|\mathbf{x}, \mathbf{y}) \leftarrow \frac{\widehat{\Pi}_{MMD^2}(0|\mathbf{x}, \mathbf{y})}{\widehat{\Pi}_{MMD^2}(0)}$   
12:  $\widehat{Str} \leftarrow 0$   
13: **for**  $i \leftarrow 0$  to  $M - 1$  **do**  
14:  $\widehat{d}_{i/M} \leftarrow quantile(\{MMD_{BNP_r}^2(F_1^{pri}, F_2)\}_{r=1}^\ell, i/M)$   $\triangleright$  The estimation of the  $i/M$ -th  
quantile of  $MMD_{BNP}^2(F_1^{pri}, F_2)$   
15:  $\widehat{d}_{(i+1)/M} \leftarrow quantile(\{MMD_{BNP_r}^2(F_1^{pri}, F_2)\}_{r=1}^\ell, (i+1)/M)$   
16:  $\widehat{RB}_{MMD^2}(\widehat{d}_{i/M}|\mathbf{x}, \mathbf{y}) \leftarrow \frac{\widehat{\Pi}_{MMD^2}(\widehat{d}_{(i+1)/M}|\mathbf{x}, \mathbf{y}) - \widehat{\Pi}_{MMD^2}(\widehat{d}_{i/M}|\mathbf{x}, \mathbf{y})}{\widehat{\Pi}_{MMD^2}(\widehat{d}_{(i+1)/M}) - \widehat{\Pi}_{MMD^2}(\widehat{d}_{i/M})}$   
17: **if**  $\widehat{RB}_{MMD^2}(\widehat{d}_{i/M}|\mathbf{x}, \mathbf{y}) \leq \widehat{RB}_{MMD^2}(0|\mathbf{x}, \mathbf{y})$  **then**  
18:  $\widehat{Str} = \widehat{Str} + [\widehat{\Pi}_{MMD^2}(\widehat{d}_{(i+1)/M}|\mathbf{x}, \mathbf{y}) - \widehat{\Pi}_{MMD^2}(\widehat{d}_{i/M}|\mathbf{x}, \mathbf{y})]$   
19: **end if**  
20: **end for**  
21: **return**  $\widehat{Str}$

---

## 5. Embedding the Semi-BNP Test in Learning GANs

### 5.1 Architecture

Various GAN architectures can be found in the literature to model complex high-dimensional distributions. However, we consider the original architecture of GANs proposed by Goodfellow et al. (2014), with the difference that here only the generator is considered as a neural network and the discriminator  $D$  is formed as the semi-BNP two-sample test.

Specifically, we follow Goodfellow et al. (2014) to consider the generator  $G_{\mathbf{w}}$  as a multi-layer neural network with parameters  $\mathbf{w}$ , rectified linear units activation function for each hidden layer, and a sigmoid function for the last layer (output layer). The generator receives a noise vector  $\mathbf{U} = (U_1, \dots, U_p)$  as its input nodes, where  $p < d$ , and each element of  $\mathbf{U}$  is independently drawn from the same distribution  $F_U$ . A realistic sample here is the output of the network  $G_{\mathbf{w}}$  in data space  $\mathbb{R}^d$  based on updating  $\mathbf{w}$  by optimizing the objective function

$$\arg \max_{\mathbf{w}} \text{RB}_{MMD^2}(F_{data}, F_{G_{\mathbf{w}}})(0|\mathbf{X}_1, \dots, \mathbf{X}_n),$$

where,  $\mathbf{X}_1, \dots, \mathbf{X}_n \sim F_{data}$ . In fact, our desired discriminator calculates the RB ratio and the generator should attempt to maximize this value. This is equivalent to the generator trying to minimize the posterior-based MMD measure in the numerator of the RB ratio, when the *a priori* term is considered fixed in the denominator of the RB ratio. Hence, the problem should be changed to optimize the objective function  $\arg \min_{\mathbf{w}} MMD_{BNP}^2(F_{data}^{pos}, F_{G_{\mathbf{w}}})$ . For any differentiable kernel function  $k(\cdot, \cdot)$ , this optimization is performed by computing

the following gradient based on samples from  $F_{data}|\mathbf{X}_1, \dots, \mathbf{X}_n \sim DP(a+n, H^*)$ , as

$$\frac{\partial MMD_{BNP}^2(F_{data}^{pos}, F_{G_{\mathbf{w}}})}{\partial \mathbf{w}_i} = \sum_{\ell=1}^N \sum_{t=1}^m \left\{ \frac{\partial}{\partial \mathbf{Y}_t} \left[ -\frac{2}{m} \sum_{t=1}^m J_{\ell, N}^* k(\mathbf{V}_\ell^*, \mathbf{Y}_t) + \frac{1}{Nm^2} \sum_{t, t'=1}^m k(\mathbf{Y}_t, \mathbf{Y}_{t'}) \right] \frac{\partial \mathbf{Y}_t}{\partial \mathbf{w}} \right\}, \quad (19)$$

where,  $\mathbf{Y}_t = G_{\mathbf{w}}(\mathbf{U}_t)$ ,  $\mathbf{U}_t = (U_{t1}, \dots, U_{tp})$ , and  $U_{ti}$ 's are generated from a distribution  $F_U$ , for  $t = 1, \dots, m$ , and  $i = 1, \dots, p$ . Then, the backpropagation method is applied for calculating partial derivatives  $\frac{\partial \mathbf{Y}_t}{\partial \mathbf{w}}$  to update the parameters of  $G_{\mathbf{w}}$ .

However, Li et al. (2015, Equation 8) remarked that considering the square root of the MMD measure given by (1) in the cost function of frequentist GANs is more efficient than using (1) to train network  $G_{\mathbf{w}}$ . They mentioned that since the gradient of  $\sqrt{MMD^2(F_{data}, F_{G_{\mathbf{w}}})}$  with respect to  $\mathbf{w}$  is the product of  $\gamma_1 = \frac{1}{2\sqrt{MMD^2(F_{data}, F_{G_{\mathbf{w}}})}}$  and  $\gamma_2 = \frac{\partial MMD^2(F_{data}, F_{G_{\mathbf{w}}})}{\partial \mathbf{w}}$ , then  $\gamma_1$  forces the value of the gradient to be relatively large, even if both  $MMD^2(F_{data}, F_{G_{\mathbf{w}}})$  and  $\gamma_2$  are small. This can prevent the vanishing gradient, which improves the learning of the parameters of  $G_{\mathbf{w}}$  in the early layers of this network. We consider this point in order to improve our semi-BNP objective function:

$$\arg \min_{\mathbf{w}} MMD_{BNP}(F_{data}^{pos}, F_{G_{\mathbf{w}}}). \quad (20)$$

Algorithm 2 provides steps for implementing the semi-BNP GAN.

Let  $\mathbf{w}^*$  be the optimized parameter of  $G_{\mathbf{w}}$  that minimizes  $MMD_{BNP}(F_{data}^{pos}, F_{G_{\mathbf{w}}})$ . Since  $MMD_{BNP}(F_{data}^{pos}, F_{G_{\mathbf{w}}})$  can be viewed as a semi-BNP estimation of (1), one may be interested in assessing the error of this estimation. The next lemma addresses this concern by presenting a stochastic bound for the estimation error.

**Lemma 6** *Let  $\mathcal{W}$  be the parameter space for  $G_{\mathbf{w}}$  and  $\mathbf{w}^* \in \mathcal{W}$  be the value that optimizes the objective function (20). Assume that  $F_{data} \sim DP(a, H)$  and  $k(\cdot, \cdot)$  be any continuous kernel function with feature space corresponding to a universal RKHS such that  $k(\mathbf{z}, \mathbf{z}') < K$ , for any  $\mathbf{z}, \mathbf{z}' \in \mathbb{R}^d$ . Then, for a given sample  $\mathbf{X}_1, \dots, \mathbf{X}_n$  from distribution  $F_{data}$  and any  $\epsilon > 0$ , with a probability at least  $1 - 2 \exp \frac{-\epsilon^2 Nm}{2K(N+m)}$ ,*

$$\left| \lim_{n \rightarrow \infty} MMD_{BNP}(F_{data}^{pos}, F_{G_{\mathbf{w}^*}}) - MMD(F_{data}, F_{G_{\mathbf{w}'}}) \right| \leq h(N, m, \epsilon) + |\Delta|,$$

where,  $h(N, m, K, \epsilon) = \frac{2\sqrt{K}(\sqrt{N} + \sqrt{m})/\sqrt{Nm} + \epsilon}{|MMD_{N, m}(F_{data}, F_{G_{\mathbf{w}^*}}) + MMD(F_{data}, F_{G_{\mathbf{w}'}})|}$ ,  $\Delta = MMD(F_{data}, F_{G_{\mathbf{w}^*}}) - MMD(F_{data}, F_{G_{\mathbf{w}'}})$ , and  $\mathbf{w}'$  be the value that minimizes  $MMD(F_{data}, F_{G_{\mathbf{w}'}})$ .

**Proof** Let  $\mathcal{L}_{BNP}^2(\mathbf{w}) = MMD_{BNP}^2(F_{data}^{pos}, F_{G_{\mathbf{w}}})$ ,  $\mathcal{L}_{N, m}^2(\mathbf{w}) = MMD_{N, m}^2(F_{data}, F_{G_{\mathbf{w}}})$ , and  $\mathcal{L}^2(\mathbf{w}) = MMD^2(F_{data}, F_{G_{\mathbf{w}}})$ . Then, for  $\mathbf{w}^* \in \mathcal{W}$ , Theorem 4(iv) implies

$$\Pr \left( \left| \lim_{n \rightarrow \infty} \mathcal{L}_{BNP}^2(\mathbf{w}^*) - \mathcal{L}^2(\mathbf{w}^*) \right| > 2\sqrt{K}(\sqrt{N} + \sqrt{m})/\sqrt{Nm} + \epsilon \right) < 2 \exp \frac{-\epsilon^2 Nm}{2K(N+m)}. \quad (21)$$



By applying factorization in (21), we have

$$\Pr \left( \left| \lim_{n \rightarrow \infty} \mathcal{L}_{BNP}(\mathbf{w}^*) - \mathcal{L}(\mathbf{w}^*) \right| > \frac{2\sqrt{K}(\sqrt{N} + \sqrt{m})/\sqrt{Nm} + \epsilon}{\left| \lim_{n \rightarrow \infty} \mathcal{L}_{BNP}(\mathbf{w}^*) + \mathcal{L}(\mathbf{w}^*) \right|} \right) < 2 \exp \frac{-\epsilon^2 Nm}{2K(N+m)}.$$

Similar to the proof of Theorem 3(ii),  $\mathcal{L}_{BNP}^2(\mathbf{w}^*) \xrightarrow{a.s.} \mathcal{L}_{N,m}^2(\mathbf{w}^*)$ , as  $n \xrightarrow{a.s.} \infty$ . The continuous mapping theorem implies

$$\Pr \left( \left| \lim_{n \rightarrow \infty} \mathcal{L}_{BNP}(\mathbf{w}^*) - \mathcal{L}(\mathbf{w}^*) \right| > h(N, m, K, \epsilon) \right) < 2 \exp \frac{-\epsilon^2 Nm}{2K(N+m)}.$$

Hence, with a probability at least  $1 - 2 \exp \frac{-\epsilon^2 Nm}{2K(N+m)}$ ,

$$\left| \lim_{n \rightarrow \infty} \mathcal{L}_{BNP}(\mathbf{w}^*) - \mathcal{L}(\mathbf{w}^*) \right| \leq h(N, m, K, \epsilon). \quad (22)$$

On the other hand, the triangle inequality implies

$$\left| \lim_{n \rightarrow \infty} \mathcal{L}_{BNP}(\mathbf{w}^*) - \mathcal{L}(\mathbf{w}') \right| \leq \left| \lim_{n \rightarrow \infty} \mathcal{L}_{BNP}(\mathbf{w}^*) - \mathcal{L}(\mathbf{w}^*) \right| + \left| \mathcal{L}(\mathbf{w}^*) - \mathcal{L}(\mathbf{w}') \right|. \quad (23)$$

Finally, the proof is concluded by considering inequality (22) in (23).  $\blacksquare$

---

**Algorithm 2** Pseudocode of training a GAN using the semi-BNP approach

---

- 1: Initialize  $a$  and  $N$
  - 2:  $r_{mn} \leftarrow$  Number of training iteration,  $n_{mb} \leftarrow$  Mini-batch size
  - 3:  $\mathbf{w}_0 \leftarrow$  An initial parameter for generator  $G_{\mathbf{w}}$ ,  $\{\mathbf{x}_\ell\}_{\ell=1}^n \leftarrow$  real dataset
  - 4: **for**  $i \leftarrow 0$  to  $r_{mb}$  **do**
  - 5:      $H \leftarrow G_{\mathbf{w}_i}$
  - 6:     Generate a random sample  $\{\mathbf{x}_\ell^{mb}\}_{\ell=1}^{n_{mb}}$  from real dataset  $\{\mathbf{x}_\ell\}_{\ell=1}^n$
  - 7:     Generate a sample of noise vector  $\{\mathbf{u}_\ell\}_{\ell=1}^{n_{mb}}$  from uniform distribution  $U(-1, 1)$
  - 8:     Generate a sample from  $F_{G_{\mathbf{w}_i}}$ , distribution of  $G_{\mathbf{w}_i}$ , as  $\{\mathbf{y}_\ell = G_{\mathbf{w}_i}(\mathbf{u}_\ell)\}_{\ell=1}^{n_{mb}}$
  - 9:     Generate a sample of size  $N$  from  $F^{pos} = F_{data} | \{\mathbf{x}_\ell^{mb}\}_{\ell=1}^{n_{mb}}$  using  $\sum_{i=1}^N J_{i,N}^* \delta_{\mathbf{v}_i^*}$  by replacing  $F_1$  by  $F_{data}$ , and  $\{\mathbf{x}_\ell^{mb}\}_{\ell=1}^{n_{mb}}$  by  $\mathbf{x}$  in step (4) of Algorithm 1.
  - 10:     Use generated samples in steps 6 and 7 to compute  $MMD_{BNP}^2(F^{pos}, F_{G_{\mathbf{w}_i}})$  given by (12).
  - 11:     Use (19) to compute the gradient:
$$\frac{\partial MMD_{BNP}(F^{pos}, F_{G_{\mathbf{w}_i}})}{\partial \mathbf{w}_i} = \frac{1}{2\sqrt{MMD_{BNP}^2(F^{pos}, F_{G_{\mathbf{w}}})}} \frac{\partial MMD_{BNP}^2(F^{pos}, F_{G_{\mathbf{w}}})}{\partial \mathbf{w}}.$$
  - 12:     Use backpropagation for calculating partial derivatives  $\frac{\partial G_{\mathbf{w}_1}(\mathbf{u}_\ell)}{\partial \mathbf{w}_i}$  in the previous step to update parameter  $\mathbf{w}_i$ .
  - 13: **end for**
  - 14: **return**  $\mathbf{w}^*$       $\triangleright$  An optimized parameter for  $G_{\mathbf{w}}$  that minimizes the cost function.
- 

## 5.2 Kernel Settings

In our method, we choose to use the standard RBF kernel as its feature space corresponds to a universal RKHS. Dziugaite et al. (2015); Li et al. (2015) and Li et al. (2017) used the

Gaussian kernel in training MMD-GANs because of its simplicity and good performance. Dziugaite et al. (2015) also evaluated some other RBF kernels such as the Laplacian and rational quadratic kernels to compare the results of the MMD-GANs with those obtained based on using Gaussian kernels. They found the best performance by applying the Gaussian kernel in the MMD cost function.

Hence, we consider the Gaussian kernel function in our proposed procedure. To choose the bandwidth parameter  $\sigma$ , we follow the idea of considering a set of fixed values of  $\sigma$ 's such as  $\{\sigma_1, \dots, \sigma_T\}$ , then compute the mixture of Gaussian kernels  $k(\cdot, \cdot) = \sum_{t=1}^T k_{G_{\sigma_t}}(\cdot, \cdot)$ , to consider in (12). For each  $\sigma(t)$ ,  $0 \leq k_{G_{\sigma_t}}(\cdot, \cdot) \leq 1$ ; hence,  $0 \leq k(\cdot, \cdot) \leq T$ , which satisfies to the theoretical results presented in the paper. As it is mentioned in Section 3.3, this choice reflects a good performance in training MMD-GANs.

### 5.3 An MMD Matching Score Function

We first revisit the MBM method used in the matching score function (6) proposed by Zhang (2021) who argued that considering  $n!$  permutations in (6) is time-consuming, an optimal permutation chosen by the MBM algorithm is instead considered to compute  $MCS$ . To continue the discussion, we need to briefly review some of the main concepts in the bipartite graph theory.

Let a bipartite graph be denoted by  $\mathcal{B} = (U, V, E)$ , where  $E$  is the set of all edges connecting the nodes in the set  $U$  to the nodes in the set  $V$ . A bipartite matching is a subset  $E_{MBM} \subseteq E$  for  $\mathcal{B}$  such that no edges in  $E_{MBM}$  share an endpoint (Lovász and Plummer, 1986). An MBM is a bipartite matching with the maximum number of edges such that if an edge is added to its edges set, the bipartite graph is no longer a matching. It should be noted that more than one maximum matching can exist for a bipartite graph  $\mathcal{B}$  and then MBMs are not unique in such graphs (Jia et al., 2022). For instance, when the number of nodes in sets  $U$  and  $V$  is the same, there could be  $n!$  MBMs for bipartite graph  $\mathcal{B}$ .

Now, consider  $U$  as the set of the real dataset  $\mathbf{X}_1, \dots, \mathbf{X}_n$  and  $V$  as the set of  $\mathbf{Y}_1(\mathbf{w}^*), \dots, \mathbf{Y}_n(\mathbf{w}^*)$ , drawn from the trained generator  $G_{\mathbf{w}^*}$ , in the matching score procedure given by Section 3.4. Since each permutation of nodes in  $V$  must be compared to the elements of  $U$ , there are  $n!$  MBMs between  $U$  and  $V$ . To be clearer, all MBM graphs are given for  $n = 3$  by Figure 1. It is worth mentioning that MBM algorithms mentioned in Section 3.4 often randomly output one of  $n!$  possible MBMs. Hence, we prefer to use the term ‘‘random permutation’’ as opposed to using the term ‘‘optimal permutation’’ in the procedure proposed by Zhang (2021). On the other hand, the MBM may not be a particularly informative score to demonstrate the similarity between the two samples. For example, for  $i = 1, \dots, n$ , let  $\mathbf{X}_i$  be a handwritten image for the number  $i$ . Also, assume that samples  $\mathbf{Y}_i(\mathbf{w}^*)$ 's, produced by the trained generator, which has high resolution and great diversity. However, a randomly chosen MBM may connect none of the generated data to its corresponding data, or very few  $\mathbf{Y}_i(\mathbf{w}^*)$  to the corresponding  $\mathbf{X}_i(\mathbf{w}^*)$ . In this case,  $s(\mathbf{X}_i, \mathbf{Y}_{t(i)}(\mathbf{w}^*))$  in (6) might have a low value leading to a poor  $MCS$ , while the observed generated samples may in fact exhibit good performance in terms of diversity and resolution.

Instead of considering only a random MBM, it is more reasonable to consider several bipartite graphs constructed based on resampling from  $\{\mathbf{X}_i\}_{i=1}^n$  and  $\{\mathbf{Y}_i(\mathbf{w}^*)\}_{i=1}^n$  with

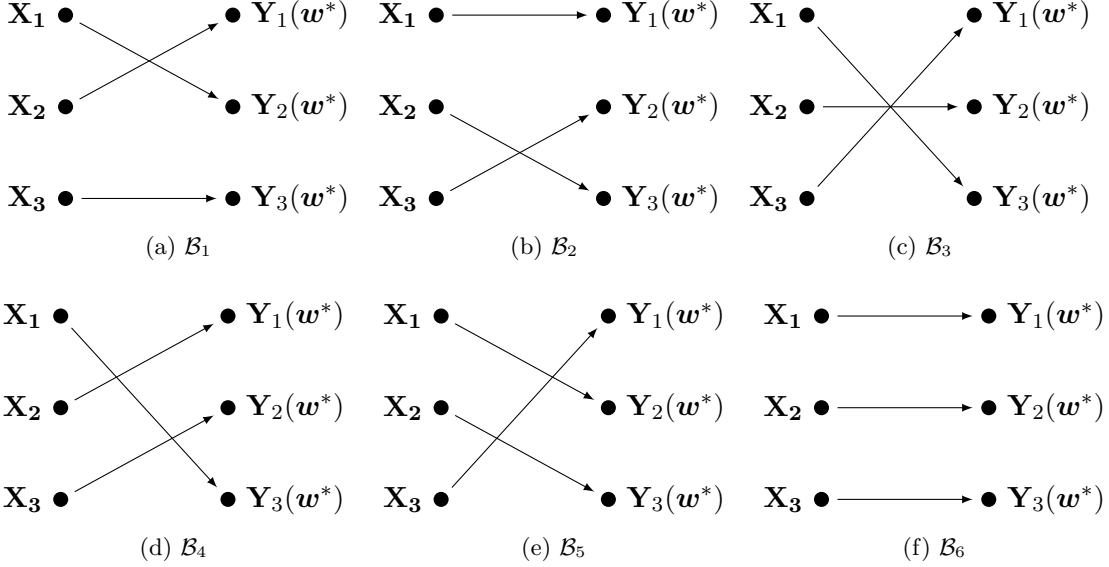


Figure 1: All possible MBMs between real and generated datasets with the same sample size  $n = 3$ .

smaller sample sizes than  $n$  and then collect a random MBM in each bipartite (mini-batch strategy). In this case, more matchings are considered, which provides more comparison for checking the quality of the generated samples. However, the implementation of MBM algorithms will be time-consuming and also most of the data information will still be lost due to neglecting to consider all matchings.

To develop a stronger method for evaluating the differences between real and generated data manifolds, we propose using the MMD dissimilarity measure instead of using the cosine similarity measure as follows: For  $i = 1, \dots, r_{mb}$ , let  $\{\mathbf{X}_{i_j}\}_{j=1}^{n_{mb}}$  and  $\{\mathbf{Y}_{i_j}(\mathbf{w}^*)\}_{j=1}^{n_{mb}}$  be two samples drawn, respectively, from the real dataset  $\mathbf{X}_1, \dots, \mathbf{X}_n$  and the generated dataset  $\mathbf{Y}_1(\mathbf{w}^*), \dots, \mathbf{Y}_n(\mathbf{w}^*)$  with the same sample size  $n_{mb} < n$ . Then, we define the MMD-based matching score as

$$MMDS = \max_{i \in \{1, \dots, r_{mb}\}} MMD_{n_{mb}, n_{mb}}^2(F_{data}(i), F_{G_{\mathbf{w}^*}}(i)), \quad (24)$$

where,  $MMD_{n_{mb}, n_{mb}}^2(F_{data}(i), F_{G_{\mathbf{w}^*}}(i))$  is the MMD approximation given by (2) using samples  $\{\mathbf{X}_{i_j}\}_{j=1}^{n_{mb}}$  and  $\{\mathbf{Y}_{i_j}(\mathbf{w}^*)\}_{j=1}^{n_{mb}}$  (mini-batch samples). Our proposed matching score returns the maximum value of the MMD approximation between a subset of the real and a subset of the generated dataset with the same size  $n_{mb}$  (mini-batch sample size) over  $r_{mb}$  re-samplings (mini-batch iteration). According to Equation (2), all components of mini-batch samples are compared together in the MMD measure, which provides a comprehensive assessment between subsets of the data in each iteration. Eventually, it is obvious smaller values of  $MMDS$  indicate better quality and more diversity of the generated samples.

## 6. Experimental Investigation

In this section, we empirically investigate our proposed methods through comprehensive numerical studies in the following two subsections, which demonstrate the superior performance of our proposed semi-BNP test as a standalone test as well as an embedded discriminator for the semi-BNP GAN.

### 6.1 The Semi-BNP Test

To provide a comprehensive study of test performance evaluation, we consider some major representative examples in two-sample comparison problems. For this, let  $\mathbf{y}_1, \dots, \mathbf{y}_n$  be a sample generated from  $F_2 = N(\mathbf{0}_d, I_d)$  and  $\mathbf{x}_1, \dots, \mathbf{x}_n$  be a sample generated from each below distributions:

1. **No differences:**  $F_1 = N(\mathbf{0}_d, I_d)$ ,
2. **Mean shift:**  $F_1 = N(\mathbf{0.5}_d, I_d)$ ,
3. **Skewness:**  $F_1 = LN(\mathbf{0}_d, B_d)$ ,
4. **Mixture:**  $F_1 = \frac{1}{2}N(-\mathbf{1}_d, I_d) + \frac{1}{2}N(\mathbf{1}_d, I_d)$ ,
5. **Variance shift:**  $F_1 = N(\mathbf{0}_d, 2I_d)$ ,
6. **Heavy tail:**  $F_1 = t_3(\mathbf{0}_d, I_d)$ ,
7. **Kurtosis:**  $F_1 = LG(\mathbf{0}_d, I_d)$ ,

where  $N(\cdot, \cdot)$  denotes a normal distribution,  $LN(\cdot, \cdot)$  denotes a lognormal distribution,  $t_3(\cdot, \cdot)$  denotes a  $t$ -distribution with 3 degrees of freedom, and  $LG(\cdot, \cdot)$  denotes a logistic distribution, where  $B_d$  is an  $d \times d$  matrix with 0.25 on the main diagonal and 0.2 off the diagonal,  $\mathbf{c}_d$  is a  $d$ -dimensional column vectors of  $c$ 's, and  $I_d$  is a  $d \times d$  identical matrix. In all distribution notations, the first component represents the mean vector and the second component represents the covariance matrix.

To implement the test we set  $N = \ell = 1000$  and  $M = 20$  in Algorithm 1. We first considered the mixture of six Gaussian kernels corresponding to the suggested bandwidth parameters 1, 5, 10, 20, 40, and 80 by Li et al. (2015). We found that although this choice can provide good results in training GANs, it does not provide satisfactory results in hypothesis testing problems.

Instead of using a mixture of several Gaussian kernels, we propose choosing a specific value for the bandwidth parameter that maximizes the area under the receiver operating characteristic curve (AUC) empirically. In a binary classifier, which can also be thought of as a two-sample test assessing whether two samples are distinguishable or not, the receiver operating characteristic (ROC) curve is a plot of true positive rates (sensitivity) against the false positive rates (1-specificity) based on different choices of threshold to display the performance of the test. The positive term refers to rejecting  $\mathcal{H}_0$  in (14), while, the negative term refers to failing to reject  $\mathcal{H}_0$ . The false positive and false negative rates are equivalent to type I and type II errors, respectively. Hence, a higher AUC indicates a better diagnostic ability of a binary test. It should be noted that since we consider  $i_0/M = 0.05$  to estimate the RB ratio, the values of  $RB$  can vary between 0 and 20. Therefore, in computing the AUC for the semi-BNP test, the threshold should vary from 0 to 20. More details for plotting the ROC and computing the AUC are provided by Algorithm 3 in Appendix B. The ROC curves and AUC values of the synthetic examples are given in Figure 2 for the sample size  $n = 50$ ,  $d = 60$ ,  $a = 25$ , and various values of the bandwidth parameter. The red diagonal line represents the random classifier. A ROC curve located higher than the diagonal line indicates better test performance and vice versa. It is obvious from figure 2 that the best test performance (AUC = 1) is achieved for the bandwidth parameter 80.

Another test of interest is to assess the effect of different hyperparameters settings for  $a$  and  $H$  through simulation studies to follow our proposed theoretical convergence results. To do this, we generate 100 60-dimensional samples of sizes  $n = 50$  from both  $F_1 = t_3(\mathbf{0}_{60}, I_{60})$  and  $F_2 = N(\mathbf{0}_{60}, I_{60})$  and represent the result of the semi-BNP test by Figure 3 for two choices of the base measure  $H$  ( $H = F_2$  and  $H = LG(\mathbf{0}_{60}, I_{60})$ ) and various values of  $a$  ( $a = 1, \dots, 1000$ ). In this figure, the solid line represents the average of the RB and

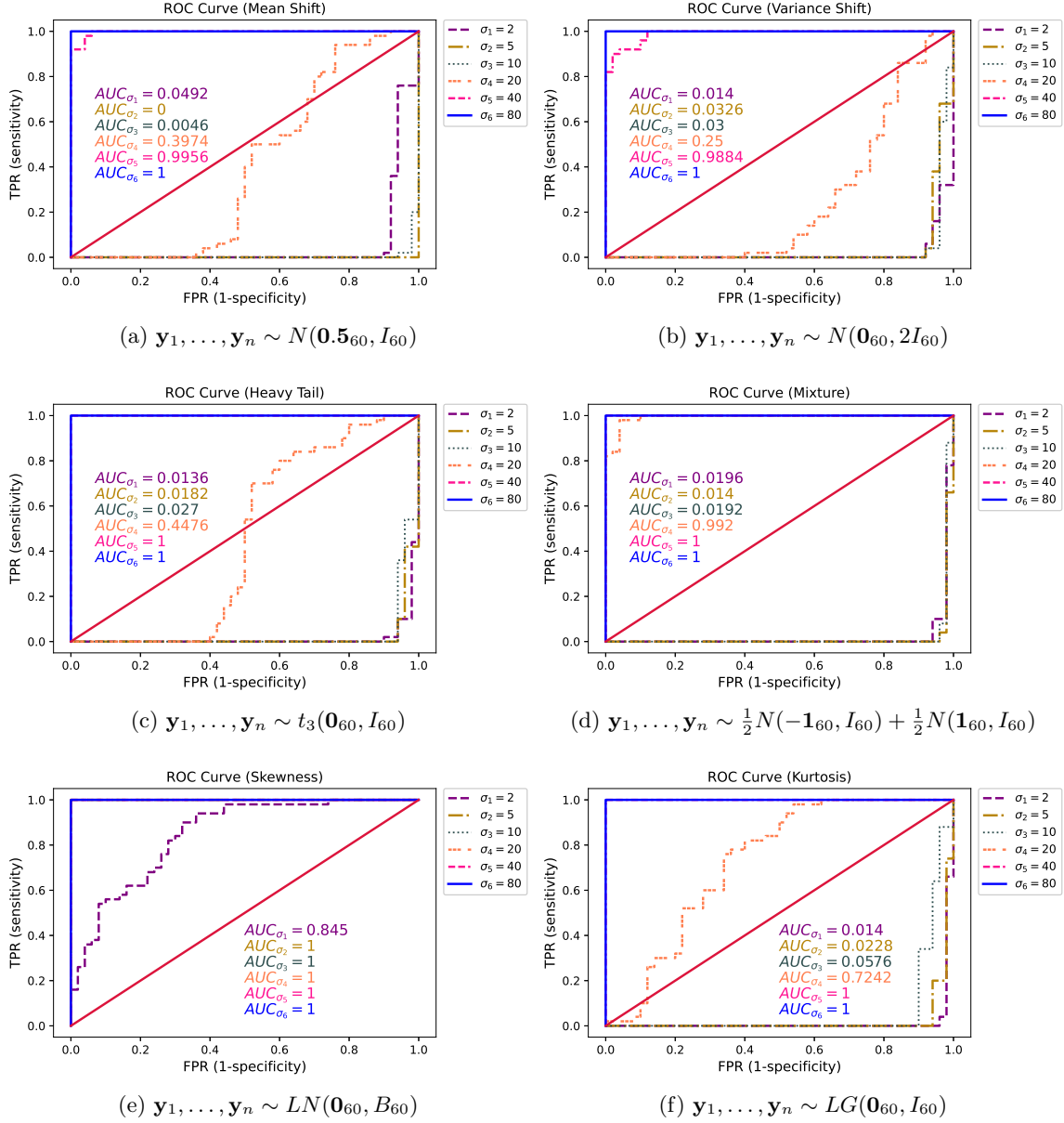


Figure 2: The ROC curves and AUC values of the BNP-MMD test for  $\mathbf{x}_1, \dots, \mathbf{x}_n \sim N(\mathbf{0}_{60}, I_{60})$  with various bandwidth parameters  $\sigma = 2, 5, 10, 20, 40, 80$ .

the filled area around the line indicates a 95% confidence interval of the RB over the 100 samples. Figure 3-a clearly shows that by choosing  $H \neq F_2$ , the test wrongly accepts the null hypothesis. It is because the prior does not support the null hypothesis mentioned earlier when presenting the RB ratio in Section 4. On the other hand, when  $H = F_2$ , Figure 3-b shows good performance for the test at  $a = n/2$ . Failing to reject  $\mathcal{H}_0$  for small values of  $a$  is due to the lack of sufficient support from the null hypothesis by the prior. We remark that the value of  $a$  determines the concentration of the prior  $F^{pri}$  around  $H$ , thus it is obvious that for small values of  $a$ , the test does not perform well. It should also be noted that for any choices of  $H$  in Figure 3, the ability of the test to evaluate the null hypothesis is reduced by letting  $a$  go to infinity, which can be concluded by Corollary 2(ii) and Theorem 4(i).

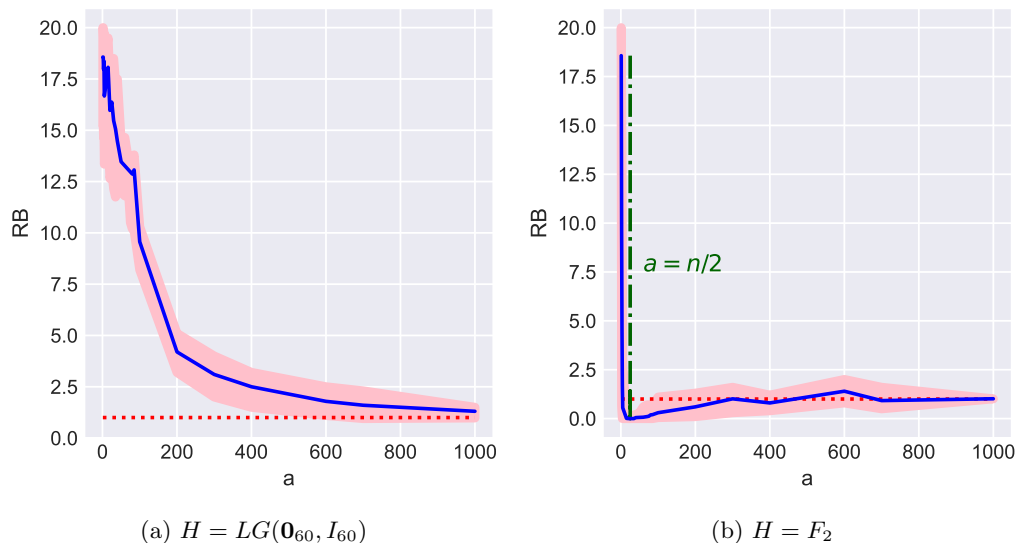


Figure 3: The solid line represents the average of the RB and the pink area represents a 95% confidence interval of the RB over the 100 samples with various choices of  $H$  and  $a$  for the heavy tail example. The lower and upper bounds are the 2.5% and 97.5% quantiles of the RB, respectively. The red dotted line represents  $RB = 1$ .

Now, for a more comprehensive investigation, the average of RB and its relevant strength over the 100 samples are presented in Table 1 for  $n = 30, 50$ . The results of the BNP-energy test of Al-Labadi et al. (2022a) are also given in Table 1 and Figure 4 to compare the proposed method with its Bayesian competitor. Figure 4 provides the plot of the proportion of rejecting  $\mathcal{H}_0$  over the 100 samples for both mentioned Bayesian tests in different data dimensions. This Figure shows the better performance of the semi-BNP kernel-based test than the BNP-energy test, especially in variance shift, heavy tail, and kurtosis examples.

To compare the Bayesian and frequentist nonparametric (FNP) tests, the  $p$ -values of the frequentists counterparts corresponding to each Bayesian test are presented in Table 1. AUC values of all tests are also given to facilitate comparison between tests. Generally, the Bayesian tests reflect better performances than their frequentist counterparts in lower

Table 1: The average of RB, the average of its strength (Str ), and the relevant AUC out of 100 replications based on using  $a = 25$ ,  $\ell = N = 1000$ ,  $M = 20$ , and bandwidth parameter  $\sigma = 80$  in RBF kernel for two sample of data with  $n = 30, 50$ .

Example	$d$	BNP								FNP							
		MMD				Energy				MMD				Energy			
		RB(Str)		AUC		RB(Str)		AUC		P.value		AUC		P.value		AUC	
		30	50	30	50	30	50	30	50	30	50	30	50	30	50	30	50
No differences	1	2.08(0.62)	2.41(0.67)	/	/	1.78(0.59)	1.91(0.55)	/	/	0.50	0.45	/	/	0.50	0.49	/	/
	5	4.06(0.77)	6.91(0.76)	/	/	3.46(0.65)	5.99(0.73)	/	/	0.48	0.50	/	/	0.54	0.52	/	/
	10	6.21(0.78)	10.74(0.79)	/	/	5.92(0.67)	10.42(0.76)	/	/	0.50	0.51	/	/	0.54	0.47	/	/
	20	9.62(0.80)	16.02(0.83)	/	/	8.24(0.73)	14.76(0.78)	/	/	0.46	0.50	/	/	0.51	0.50	/	/
	40	13.07(0.88)	18.85(0.97)	/	/	11.56(0.75)	17.58(0.84)	/	/	0.51	0.49	/	/	0.53	0.46	/	/
	60	14.09(0.87)	19.71(1)	/	/	13.38(0.81)	18.51(0.93)	/	/	0.52	0.46	/	/	0.50	0.48	/	/
	80	15.2(0.89)	19.57(1)	/	/	14.16(0.87)	19.10(1)	/	/	0.46	0.47	/	/	0.53	0.56	/	/
	100	15.83(0.91)	19.74(1)	/	/	14.84(0.92)	19.31(1)	/	/	0.48	0.46	/	/	0.49	0.55	/	/
Mean shift	1	0.76(0.24)	0.40(0.09)	0.82	0.96	0.67(0.21)	0.45(0.11)	0.87	0.90	0.15	0.05	0.86	0.91	0.19	0.12	0.79	0.86
	5	0.21(0.03)	0.07(0)	0.99	0.99	0.28(0.04)	0.09(0.01)	0.98	1	0.01	0.002	1	0.98	0.02	0.004	0.97	0.97
	10	0.09(0.01)	0.05(0)	1	1	0.17(0.05)	0.02(0)	0.98	1	0.001	0.001	1	1	0.006	0.004	0.98	1
	20	0.09(0.01)	0(0)	1	1	0.09(0.01)	0(0)	1	1	0.001	0.001	1	1	0.004	0.004	1	1
	40	0.08(0)	0(0)	1	1	0.06(0.02)	0(0)	1	1	0.001	0.001	1	1	0.004	0.004	1	1
	60	0.09(0.03)	0(0)	1	1	0.07(0.04)	0(0)	1	1	0.001	0.001	1	1	0.004	0.004	1	1
	80	0.06(0.02)	0(0)	1	1	0.05(0.03)	0(0)	1	1	0.001	0.001	1	1	0.004	0.004	1	1
	100	0.04(0.01)	0(0)	1	1	0.03(0)	0(0)	1	1	0.001	0.001	1	1	0.004	0.004	1	1
Skewness	1	0.01(0)	0(0)	0.99	1	0.07(0)	0(0)	0.99	1	0.009	0.001	0.98	1	0.007	0.004	0.94	1
	5	0(0)	0(0)	1	1	0(0)	0(0)	1	1	0.001	0.001	1	1	0.004	0.004	1	1
	10	0(0)	0(0)	1	1	0(0)	0(0)	1	1	0.001	0.001	1	1	0.004	0.004	1	1
	20	0(0)	0(0)	1	1	0(0)	0(0)	1	1	0.001	0.001	1	1	0.004	0.004	1	1
	40	0(0)	0(0)	1	1	0(0)	0(0)	1	1	0.001	0.001	1	1	0.004	0.004	1	1
	60	0(0)	0(0)	1	1	0(0)	0(0)	1	1	0.001	0.001	1	1	0.004	0.004	1	1
	80	0(0)	0(0)	1	1	0(0)	0(0)	1	1	0.001	0.001	1	1	0.004	0.004	1	1
	100	0(0)	0(0)	1	1	0(0)	0(0)	1	1	0.001	0.001	1	1	0.004	0.004	1	1
Mixture	1	0.06(0)	0(0)	0.95	1	0.19(0.03)	0.04(0)	0.97	1	0.43	0.38	0.58	0.57	0.29	0.17	0.69	0.81
	5	0(0)	0(0)	1	1	0(0)	0(0)	1	1	0.15	0.09	0.84	0.91	0.06	0.01	0.95	1
	10	0(0)	0(0)	1	1	0(0)	0(0)	1	1	0.03	0.007	0.95	0.98	0.02	0.007	0.96	1
	20	0(0)	0(0)	1	1	0(0)	0(0)	1	1	0.002	0.001	0.96	1	0.01	0.006	1	1
	40	0(0)	0(0)	1	1	0(0)	0(0)	1	1	0.001	0.001	1	1	0.01	0.006	1	1
	60	0(0)	0(0)	1	1	0(0)	0(0)	1	1	0.001	0.001	1	1	0.006	0.009	1	1
	80	0(0)	0(0)	1	1	0(0)	0(0)	1	1	0.001	0.001	1	1	0.008	0.006	1	1
	100	0(0)	0(0)	1	1	0(0)	0(0)	1	1	0.001	0.001	1	1	0.004	0.006	1	1
Variance shift	1	0.87(0.29)	0.66(0.19)	0.81	0.93	1.10(0.36)	1.08(0.33)	0.74	0.83	0.46	0.38	0.54	0.57	0.33	0.21	0.65	0.77
	5	0.55(0.12)	0.56(0.15)	0.99	0.99	1.06(0.35)	0.99(0.32)	0.89	0.98	0.34	0.20	0.65	0.80	0.20	0.07	0.82	0.93
	10	0.44(0.11)	0.27(0.05)	0.99	1	0.87(0.24)	0.80(0.25)	0.97	1	0.14	0.03	0.85	0.97	0.10	0.02	0.89	0.97
	20	0.34(0.07)	0.08(0)	1	1	0.65(0.17)	0.60(0.13)	0.99	1	0.01	0.001	0.95	1	0.03	0.006	0.95	1
	40	0.13(0.01)	0.02(0)	1	1	0.61(0.18)	0.58(0.14)	1	1	0.001	0.001	1	1	0.01	0.004	0.98	1
	60	0.12(0.01)	0.01(0.0)	1	1	0.47(0.10)	0.45(0.11)	1	1	0.001	0.001	1	1	0.006	0.004	1	1
	80	0.17(0.01)	0(0)	1	1	0.54(0.12)	0.47(0.11)	1	1	0.001	0.001	1	1	0.005	0.004	1	1
	100	0.14(0.01)	0(0)	1	1	0.45(0.10)	0.41(0.08)	1	1	0.001	0.001	1	1	0.004	0.004	1	1
Heavy tail	1	0.93(0.28)	0.66(0.20)	0.89	0.92	1.19(0.41)	1.10(0.38)	0.70	0.78	0.43	0.39	0.57	0.56	0.39	0.36	0.59	0.62
	5	0.32(0.06)	0.37(0.08)	0.99	0.99	0.77(0.24)	0.78(0.23)	0.93	0.99	0.20	0.11	0.79	0.89	0.03	0.006	0.97	1
	10	0.35(0.08)	0.13(0.02)	0.99	1	0.61(0.16)	0.68(0.19)	0.98	1	0.06	0.007	0.92	0.98	0.09	0.01	0.90	0.97
	20	0.15(0.02)	0(0)	1	1	0.48(0.12)	0.46(0.12)	1	1	0.002	0.001	0.96	1	0.02	0.005	0.96	1
	40	0.07(0.01)	0(0)	1	1	0.25(0.04)	0.18(0.04)	1	1	0.001	0.001	1	1	0.005	0.004	1	1
	60	0.02(0)	0(0)	1	1	0.22(0.03)	0.14(0.01)	1	1	0.001	0.001	1	1	0.004	0.004	1	1
	80	0.01(0)	0(0)	1	1	0.13(0.01)	0.15(0.02)	1	1	0.001	0.001	1	1	0.004	0.004	1	1
	100	0.04(0)	0(0)	1	1	0.14(0.01)	0.09(0.01)	1	1	0.001	0.001	1	1	0.004	0.004	1	1
Kurtosis	1	0.47(0.12)	0.19(0.04)	0.89	0.98	1.09(0.37)	0.88(0.28)	0.77	0.90	0.28	0.23	0.74	0.72	0.18	0.11	0.79	0.88
	5	0.16(0.03)	0.06(0.01)	1	1	0.63(0.18)	0.41(0.09)	0.96	0.99	0.04	0.01	0.94	0.98	0.03	0.008	0.97	0.96
	10	0.02(0)	0(0)	1	1	0.35(0.08)	0.32(0.06)	0.97	1	0.001	0.001	1	1	0.007	0.004	0.96	1
	20	0(0)	0(0)	1	1	0.20(0.03)	0.18(0.02)	1	1	0.001	0.001	1	1	0.004	0.004	1	1
	40	0(0)	0(0)	1	1	0.06(0.01)	0.06(0)	1	1	0.001	0.001	1	1	0.004	0.004	1	1
	60	0(0)	0(0)	1	1	0.05(0)	0.04(0)	1	1	0.001	0.001	1	1	0.004	0.004	1	1
	80	0(0)	0(0)	1	1	0.05(0)	0.03(0)	1	1	0.001	0.001	1	1	0.004	0.004	1	1
	100	0(0)	0(0)	1	1	0.02(0)	0(0)	1	1	0.001	0.001	1	1	0.004	0.004	1	1

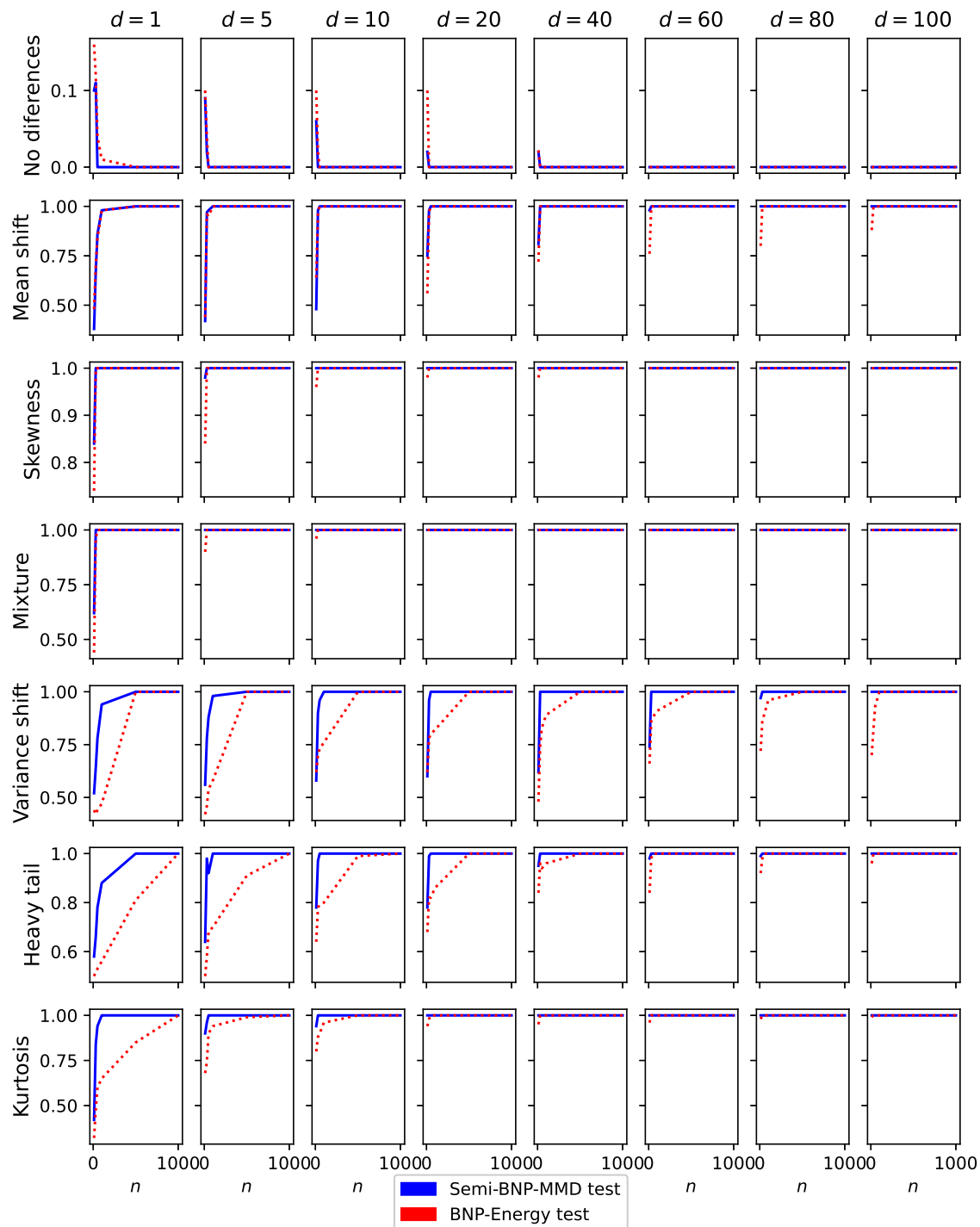


Figure 4: The proportion of rejecting  $\mathcal{H}_0$  out of 100 replications against sample of sizes  $n = 10, \dots, 1000$  based on using  $a = 25$ ,  $\ell = N = 1000$ ,  $M = 20$  for the semi-BNP-MMD (blue line) and BNP-energy (red dotted) tests.



dimensions. For instance, in the variance shift example, when  $d = 5$  and  $n = 30$ , the average of the  $RB$  and its strength for the semi-BNP-MMD test are 0.55 and 0.12, respectively, which shows strong evidence to reject the null. While the average of the  $p$ -value corresponding to the MMD frequentist test is 0.34, which shows a failure to reject the null hypothesis. The AUC value of the semi-BNP test is also 0.99 which indicates a better ability than its frequentist counterpart with an AUC of 0.82.

## 6.2 The Semi-BNP GAN

According to results reported by the previous subsection, as the semi-BNP test outperforms other competitive tests in many scenarios, we expect that embedding this test in GANs as the discriminator makes an accurate comparison to distinguish the real and fake data. We use the database of handwritten digits with 10 modes, bone marrow biopsy histopathology, human faces, and brain MRI images to analyze the model performance. Following Li et al. (2015), we consider the Gaussian neural network for the generator with four hidden layers each having rectified linear units activation function and a sigmoid function for the output layer. There are numerous methods to choose network parameters. We adopt the Bayesian optimization method, considered by Li et al. (2015), to determine the number of nodes in hidden layers and tuning parameters of the network thanks to its good performance. We also set mini-batch sizes of  $n_{mb} = 1,000$  and a mixture of six Gaussian kernels corresponding to the bandwidth parameters 1, 5, 10, 20, 40, and 80 to train networks discussed in this section.

### 6.2.1 MNIST DATASET (LECUN, 1998):

The MNIST dataset includes 60,000 handwritten digits of 10 numbers from 0 to 9 each having 784 ( $28 \times 28$ ) dimensions. This dataset is split into 50000 training and 10000 testing images and is a good example to demonstrate the performance of the method in dealing with the mode collapse problem. We use the training set to train the network. A sample from the training MNIST dataset is shown in Figure 5-a. After  $r_{mb} = 40,000$  iterations, we generate samples from the trained semi-BNP GAN using Algorithm 2 shown in Figure 5-b. The results of Li et al. (2015)<sup>2</sup> are also presented by Figure 5-c as the frequentist counterpart of our semi-BNP procedure. Based on these preliminary results, we can see that our generated images can, at least, replicate the results of Li et al. (2015) and in some cases produce sharper images. This result can also be deduced from the presented values of the score function  $MMDS$  in Table 2.

On the other hand in contrast to the semi-BNP test, we experimentally show that the semi-BNP GAN using a mixture of Gaussian kernels performs better than considering a single Gaussian kernel. In order to investigate this issue we show several samples of the trained generator using a Gaussian kernel based on different values of  $\sigma$  in Figure 6. Although the diversity of the generated image increases as the value of  $\sigma$  is increased, it is obvious that the resolution of the images in Figure 6 does not reach the image quality produced by the mixture kernel.

---

2. The implementation codes for the GAN proposed by Li et al. (2015) is available at [https://www.dropbox.com/s/anf9z1zyqi7379n/Generative-Moment-Matching-Networks-master.zip?file\\_subpath=%2FREADME.md](https://www.dropbox.com/s/anf9z1zyqi7379n/Generative-Moment-Matching-Networks-master.zip?file_subpath=%2FREADME.md)

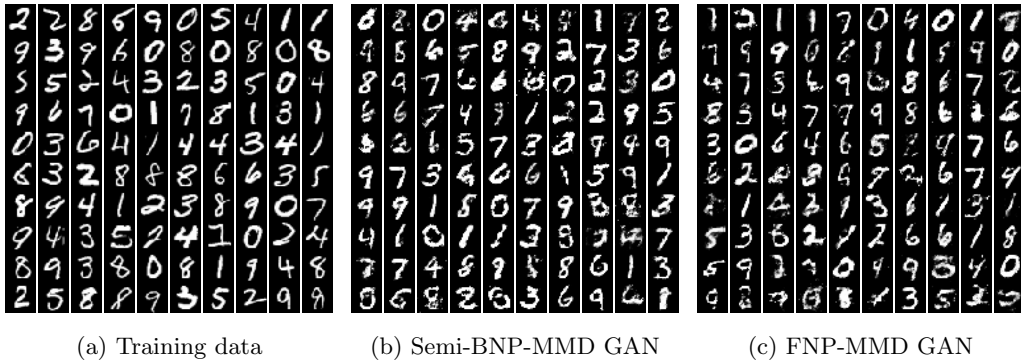


Figure 5: Generated samples of sizes  $(10 \times 10)$  from semi-BNP-MMD and MMD-FNP GAN for the MNIST dataset using a mixture of Gaussian kernels in 40,000 iterations.

In contrast to using MMD kernel-based measures, it may also be interesting to consider the energy distance in learning GANs from a BNP perspective. To address this concern, we embed the two-sample BNP-energy test of Al-Labadi et al. (2022a) in training GANs as a discriminator and showing the generated samples in Figure 7-a. This image clearly shows the inefficiency of the two-sample BNP test of Al-Labadi et al. (2022a) in training the generator. The main issue in this test procedure is treating  $F_{G_w}$  as unknown distribution to place a DP prior on it which is contrary to update parameter  $w$  in the parameterized generative neural network  $G_w$ .

One may also be interested in considering the semi-BNP-energy procedure in learning GANs which makes more sense to compare the semi-BNP-MMD results. To do this, we use the energy distance instead of the MMD in Algorithm 2. The results are presented in Figure 7-b and show blurry and unclear images with no variety, which reflect the inefficiency of using the energy distance compared to the MMD kernel-based measure.

Now, we examine the performance of the proposed GAN through additional datasets, the details of which are given below. The generated samples are shown in Figures 8. Generally, the generated images using semi-BNP GAN show better resolution than the FNP GAN. The MMD scores presented in Table 2 are also evidence to demonstrate this claim.

### 6.2.2 BONE MARROW BIOPSY DATASET (TOMCZAK AND WELLING, 2016):

The bone marrow biopsy (BMB) dataset is a collection of histopathology of BMB images corresponding to 16 patients with some types of blood cancer and anemia: 10 patients for training, 3 for testing, and 3 for validation. This dataset contains 10,800 images in the size of  $28 \times 28$  pixels, 6,800 of which are considered for the training set. The rest of the images have been divided into two sets of equal size for testing and validation. The whole dataset can be found at [https://github.com/jmtomczak/vae\\_householder\\_flow/tree/master/datasets/histopathologyGray](https://github.com/jmtomczak/vae_householder_flow/tree/master/datasets/histopathologyGray). The results based on 6800 training images are presented in Figure 8-(a-c).

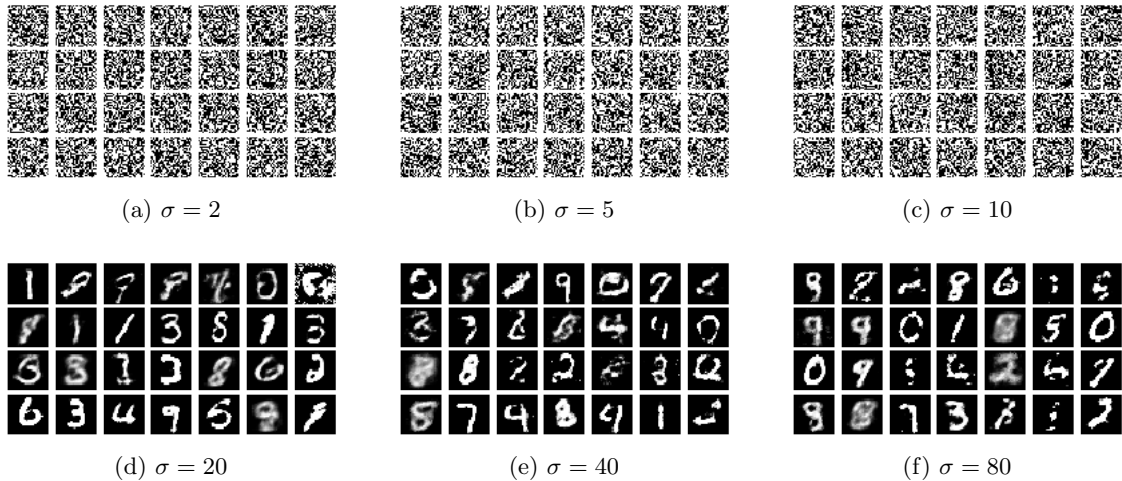


Figure 6: Generated samples from semi-BNP-MMD for the MNIST dataset using a single Gaussian kernel with various values of bandwidth parameter  $\sigma$  in 40,000 iterations.

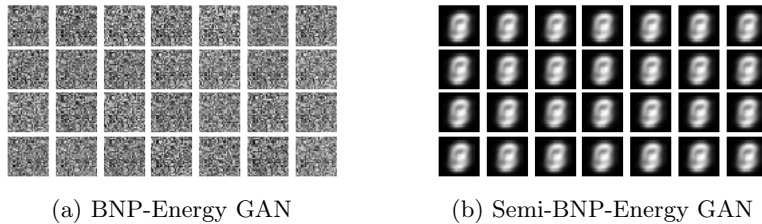


Figure 7: Generated samples from BNP-Energy and semi-BNP-Energy GAN for the MNIST dataset in 40,000 iterations.

### 6.2.3 LABELED FACES IN THE WILD DATASET (HUANG ET AL., 2008):

The labeled faces in the wild dataset (LFD) include 13,000 facial image samples with 1,024 ( $32 \times 32$ ) dimensions. The dataset is available at <https://conradsanderson.id.au/lfwcrop/>.

### 6.2.4 BRAIN TUMOR MRI DATASET (NICKPARVAR, 2021):

In the last experiment, we consider a more challenging medical dataset including brain MRI images available at <https://www.kaggle.com/dsv/2645886>. This dataset has two groups including training and testing sets. Both are classified into four classes: glioma, meningioma, no tumor, and pituitary. To train the networks, we consider all 5,712 training images. The images vary in size and have extra margins. We use a pre-processing code<sup>3</sup> to remove margins and then resize images to  $50 \times 50$  pixels. We also scale the pixel value of prepared images to range 0-1 to make the range of distribution of feature values equal and prevent any errors in the backpropagation computation.

3. <https://github.com/masoudnick/Brain-Tumor-MRI-Classification/blob/main/Preprocessing.py>

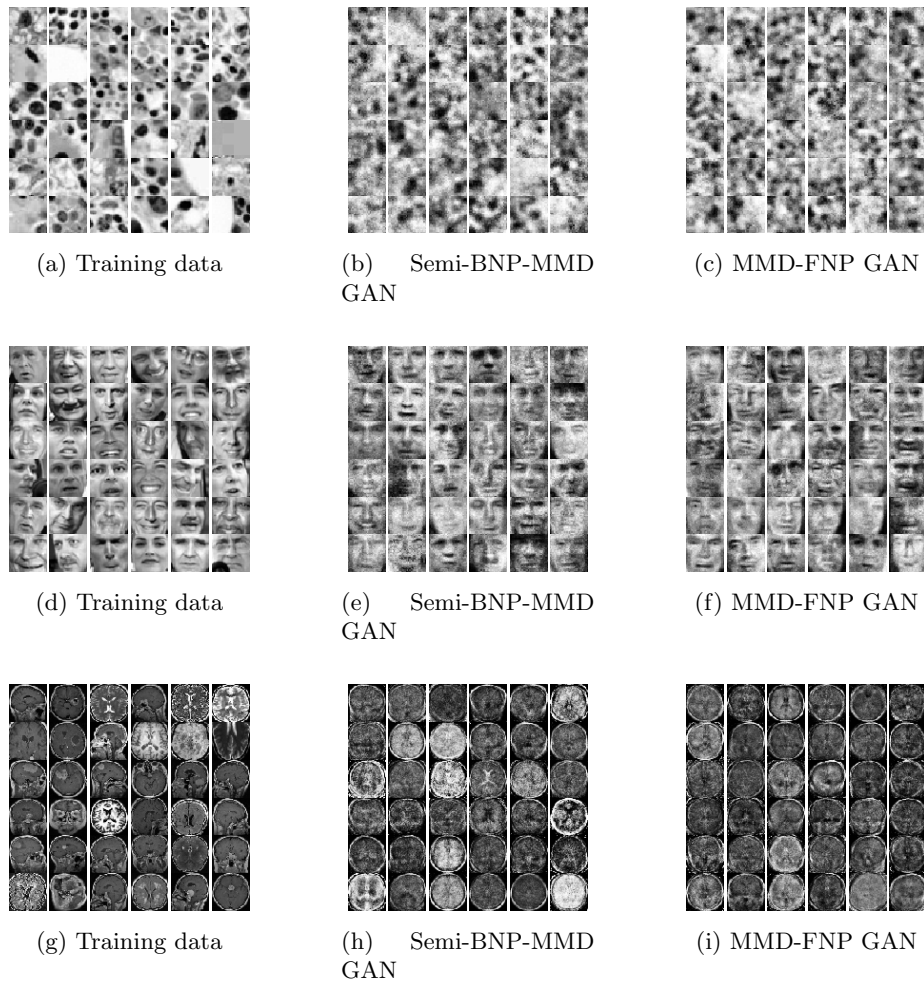


Figure 8: Generated samples of sizes  $(6 \times 6)$  from semi-BNP-MMD and MMD-FNP GAN for the BMB and LFW datasets using a mixture of Gaussian kernels in 40,000 iterations.

Table 2: The values of MMD score function for four groups of datasets considering  $n_{mb} = 500$  and  $r_{mb} = 1000$  in (24).

GAN	Dataset			
	MNIST	BMB	LFW	MRI
Semi-BNP	0.0384	0.0285	0.0281	0.1988
FNP	0.0504	0.0345	0.0422	0.2231

## 7. Conclusion

We proposed a novel approach to train GANs based on embedding a semi-BNP two-sample test as the discriminator of GAN. This discriminator was constructed by placing the DP on the training dataset and using MMD kernel-based measure to distinguish the real from

the fake data to train the parameters of the GAN generator. In addition, we provide some theoretical properties of the proposed discriminator. Next, we investigated the quality of samples generated by the proposed GAN by running a battery of experiments on some popular data sets. The results demonstrated the remarkable performance of the semi-BNP GAN in many scenarios. However, we intend to conduct a special study on generating medical images in order to improve the results in future work, which will be based on the idea proposed here.

GANs are increasingly used in medical imaging applications which are effective tools for tasks such as medical imaging reconstructions. The synthetic images generated have often been proven to be valuable especially when the original image is noisy or expensive to obtain. GANs have also been used for generating images in cross-modality synthesis problems, where we observe magnetic resonance imaging (MRI) for a given patient but want to generate computed tomography (CT) images for that same patient (Wolterink et al., 2017). This type of generative method for medical imaging can drastically reduce the time and cost of obtaining data if the quality of the synthetic examples is sufficiently high. GANs have also been used in a diagnostic capacity—for example, in detecting brain lesions in images (Alex et al., 2017).

Here, the GAN is trained by distinguishing between labeled data of brain images that contain and do not contain lesions. Then, the discriminator of the GAN is used to detect brain lesions on new images. However, GANs are far less commonly used for tasks like diagnosis. According to a survey on medical imaging research in GANs, less than 10% of the top papers surveyed were dedicated towards making diagnoses, whereas the vast majority of papers were dedicated towards generating realistic synthetic examples of medical images for further analysis (Yi et al., 2019). We believe this is because where the cost of making errors in diagnosis is immediately consequential to people, unlike other AI applications where GANs are largely used.

We plan to extend the current work by mapping the data to a lower dimensional space using an autoencoder, a dimensionality reduction model helps to reduce the noise in data and tries to optimize the cost function between the real data and fake data in the code space. Then, we will propose a 3D semi-BNP GAN in the code space to improve the ability of the GAN in generating medical datasets. The auto-encoder method should further reduce the chance of mode collapse and the 3D semi-BNP GAN will reduce the blurriness of the generated samples that may be caused by using the auto-encoder. In future work, our model will be able to generate 3D images and, hence, increase the resolution of images, especially for MRI images. We hope that our future work will make an impact in the field of medical imaging.

## Acknowledgments

The contribution of Michael Zhang was partially funded by the HKU-URC Seed Fund for Basic Research for New Staff.

## References

- L. Al-Labadi. The two-sample problem via relative belief ratio. *Computational Statistics*, 36(3):1791–1808, 2021.
- L. Al-Labadi and M. Evans. Prior-based model checking. *Canadian Journal of Statistics*, 46(3):380–398, 2018.
- L. Al-Labadi and M. Zarepour. Two-sample Kolmogorov-Smirnov test using a Bayesian nonparametric approach. *Mathematical Methods of Statistics*, 26(3):212–225, 2017.
- L. Al-Labadi, F. Fazeli Asl, and Z. Saberi. A Bayesian semiparametric Gaussian copula approach to a multivariate normality test. *Journal of Statistical Computation and Simulation*, 91(3):543–563, 2021.
- L. Al-Labadi, F. Fazeli Asl, and Z. Saberi. A Bayesian nonparametric multi-sample test in any dimension. *AStA Advances in Statistical Analysis*, 106(2):217–242, 2022a.
- L. Al-Labadi, F. Fazeli Asl, and Z. Saberi. A test for independence via Bayesian nonparametric estimation of mutual information. *Canadian Journal of Statistics*, 50(3):1047–1070, 2022b.
- L. Al-Labadi, A. Alzaatreh, and M. Evans. How to measure evidence: Bayes factors or relative belief ratios? *arXiv preprint arXiv:2301.08994*, 2023.
- V. Alex, M. S. KP, S. S. Chennamsetty, and G. Krishnamurthi. Generative adversarial networks for brain lesion detection. In *Medical Imaging 2017: Image Processing*, volume 10133, pages 113–121. SPIE, 2017.
- M. Arjovsky and L. Bottou. Towards principled methods for training generative adversarial networks. *CoRR*, abs/1701.04862, 2017. URL <http://arxiv.org/abs/1701.04862>.
- M. Arjovsky, S. Chintala, and L. Bottou. Wasserstein generative adversarial networks. In *International Conference on Machine Learning*, pages 214–223. PMLR, 2017.
- M. Bińkowski, D. J. Sutherland, M. Arbel, and A. Gretton. Demystifying MMD GANs. In *International Conference on Learning Representations*, 2018.
- L. Bondesson. On simulation from infinitely divisible distributions. *Advances in Applied Probability*, 14(4):855–869, 1982.
- K. M. Borgwardt and Z. Ghahramani. Bayesian two-sample tests. *arXiv preprint arXiv:0906.4032v1*, 2009.
- F.-X. Briol, A. Barp, A. B. Duncan, and M. Girolami. Statistical inference for generative models with maximum mean discrepancy. *arXiv preprint arXiv:1906.05944*, 2019.
- T. Che, Y. Li, A. P. Jacob, Y. Bengio, and W. Li. Mode regularized generative adversarial networks. *arXiv preprint arXiv:1612.02136*, 2016.

- J. Donahue, P. Krähenbühl, and T. Darrell. Adversarial feature learning. *arXiv preprint arXiv:1605.09782*, 2016.
- V. Dumoulin, I. Belghazi, B. Poole, O. Mastropietro, A. Lamb, M. Arjovsky, and A. Courville. Adversarially learned inference. *arXiv preprint arXiv:1606.00704*, 2016.
- G. K. Dziugaite, D. M. Roy, and Z. Ghahramani. Training generative neural networks via maximum mean discrepancy optimization. In *Proceedings of the Thirty-First Conference on Uncertainty in Artificial Intelligence*, pages 258–267, 2015.
- J. Edmonds and R. M. Karp. Theoretical improvements in algorithmic efficiency for network flow problems. *Journal of the ACM (JACM)*, 19(2):248–264, 1972.
- M. Evans. *Measuring statistical evidence using relative belief*. CRC Press, Boca Raton, FL, 2015.
- T. S. Ferguson. A Bayesian analysis of some nonparametric problems. *The Annals of Statistics*, 1(2):209–230, 1973.
- L. R. Ford and D. R. Fulkerson. Maximal flow through a network. *Canadian journal of Mathematics*, 8:399–404, 1956.
- G. García-Donato and M.-H. Chen. Calibrating Bayes factor under prior predictive distributions. *Statistica Sinica*, 15(2):359–380, 2005.
- M. G. Genton. Classes of kernels for machine learning: A statistics perspective. *Journal of machine learning research*, 2(Dec):299–312, 2001.
- I. Goodfellow, J. Pouget-Abadie, M. Mirza, B. Xu, D. Warde-Farley, S. Ozair, A. Courville, and Y. Bengio. Generative adversarial nets. *Advances in Neural Information Processing Systems*, 27:2672–2680, 2014.
- A. Gretton, K. M. Borgwardt, M. J. Rasch, B. Schölkopf, and A. Smola. A kernel two-sample test. *The Journal of Machine Learning Research*, 13(1):723–773, 2012.
- C. C. Holmes, F. Caron, J. E. Griffin, and D. A. Stephens. Two-sample Bayesian nonparametric hypothesis testing. *Bayesian Analysis*, 10:297–320, 2015.
- J. E. Hopcroft and R. M. Karp. An  $n^{5/2}$  algorithm for maximum matchings in bipartite graphs. *SIAM Journal on Computing*, 2(4):225–231, 1973.
- G. B. Huang, M. Mattar, T. Berg, and E. Learned-Miller. Labeled faces in the wild: A database for studying face recognition in unconstrained environments. In *Workshop on Faces in 'Real-Life' Images: Detection, Alignment, and Recognition*, 2008.
- H. Ishwaran and M. Zarepour. Exact and approximate sum representations for the Dirichlet process. *Canadian Journal of Statistics*, 30(2):269–283, 2002.
- H. Jeffreys. *Theory of probability*. Clarendon Press, Oxford, third edition, 1961.

- S. Jia, Y. Xi, D. Li, and H. Shao. Finding complete minimum driver node set with guaranteed control capacity. *Neurocomputing*, 2022.
- W. Jitkrittum, Z. Szabó, and A. Gretton. An adaptive test of independence with analytic kernel embeddings. In *International Conference on Machine Learning*, pages 1742–1751. PMLR, 2017.
- R. E. Kass and A. E. Raftery. Bayes factors. *Journal of the American Statistical Association*, 90(430):773–795, 1995.
- R. Kelter. Bayesian and frequentist testing for differences between two groups with parametric and nonparametric two-sample tests. *Wiley Interdisciplinary Reviews: Computational Statistics*, 13(6):e1523, 2021.
- Y. LeCun. The MNIST database of handwritten digits. <http://yann.lecun.com/exdb/mnist/>, 1998.
- C.-L. Li, W.-C. Chang, Y. Cheng, Y. Yang, and B. Póczos. MMD-GAN: Towards deeper understanding of moment matching network. *Advances in Neural Information Processing Systems*, 30, 2017.
- Y. Li, K. Swersky, and R. Zemel. Generative moment matching networks. In *International Conference on Machine Learning*, pages 1718–1727. PMLR, 2015.
- Z. Lin, A. Khetan, G. Fanti, and S. Oh. Pacgan: The power of two samples in generative adversarial networks. *Advances in Neural Information Processing Systems*, 31, 2018.
- L. Lovász and M. D. Plummer. Matching theory. *Annals of Discrete Mathematics*, 29, 1986.
- P. Muliere and L. Tardella. Approximating distributions of random functionals of ferguson-dirichlet priors. *Canadian Journal of Statistics*, 26(2):283–297, 1998.
- M. Nickparvar. Brain tumor MRI dataset, 2021. URL <https://www.kaggle.com/dsv/2645886>.
- S. Nowozin, B. Cseke, and R. Tomioka. f-GAN: Training generative neural samplers using variational divergence minimization. *Advances in Neural Information Processing Systems*, 29, 2016.
- J. N. Rouder, P. L. Speckman, D. Sun, R. D. Morey, and G. Iverson. Bayesian  $t$  tests for accepting and rejecting the null hypothesis. *Psychonomic Bulletin & Review*, 16(2):225–237, 2009.
- T. Salimans, I. Goodfellow, W. Zaremba, V. Cheung, A. Radford, and X. Chen. Improved techniques for training GANs. *Advances in Neural Information Processing Systems*, 29, 2016.
- B. Schölkopf, A. J. Smola, F. Bach, et al. *Learning with kernels: Support vector machines, regularization, optimization, and beyond*. MIT Press, 2002.



- D. Sejdinovic, B. Sriperumbudur, A. Gretton, and K. Fukumizu. Equivalence of distance-based and RKHS-based statistics in hypothesis testing. *Annals of Statistics*, pages 2263–2291, 2013.
- J. Sethuraman. A constructive definition of Dirichlet priors. *Statistica Sinica*, pages 639–650, 1994.
- J. M. Tomczak and M. Welling. Improving variational auto-encoders using householder flow. *arXiv preprint arXiv:1611.09630*, 2016.
- J. M. Wolterink, A. M. Dinkla, M. H. Savenije, P. R. Seevinck, C. A. van den Berg, and I. Išgum. Deep MR to CT synthesis using unpaired data. In *International Workshop on Simulation and Synthesis in Medical Imaging*, pages 14–23. Springer, 2017.
- X. Yi, E. Walia, and P. Babyn. Generative adversarial network in medical imaging: A review. *Medical Image Analysis*, 58:101552, 2019.
- M. Zarepour and L. Al-Labadi. On a rapid simulation of the Dirichlet process. *Statistics & Probability Letters*, 82(5):916–924, 2012.
- K. Zhang. On mode collapse in generative adversarial networks. In *Artificial Neural Networks and Machine Learning – ICANN 2021*, pages 563–574, Cham, 2021. Springer International Publishing. ISBN 978-3-030-86340-1.
- Q. Zhang, V. Wild, S. Filippi, S. Flaxman, and D. Sejdinovic. Bayesian kernel two-sample testing. *Journal of Computational and Graphical Statistics*, pages 1–24, 2022.
- F. Zhao, C. Lei, Q. Zhao, H. Yang, G. Ling, J. Liu, H. Zhou, and H. Wang. Predicting the property contour-map and optimum composition of Cu-Co-Si alloys via machine learning. *Materials Today Communications*, 30:103138, 2022.

## A. Theoretical Properties of the DP Approximation

**Proposition 7** For a non-negative real value  $a$  and fixed probability distribution  $H$ , let  $F_1^{pri} := F_1 \sim DP(a, H)$  and  $(J_{1,N}, \dots, J_{N,N}) \sim \text{Dirichlet}(\frac{a}{N}, \dots, \frac{a}{N})$  be the weights in the approximation of  $F^{pri}$ , given by Ishwaran and Zarepour (2002). Then, as  $a \rightarrow \infty$ ,

- i.  $J_{\ell,N} \xrightarrow{a.s.} \frac{1}{N}$ , for any  $\ell \in \{1, \dots, N\}$ ,
- ii.  $J_{\ell,N} J_{t,N} \xrightarrow{a.s.} \frac{1}{N^2}$ , for any  $\ell, t \in \{1, \dots, N\}$ , where  $\ell \neq t$  and “ $a.s.$ ” denotes the almost surely convergence.

**Proof** Since  $E_{F_1^{pri}}(J_{\ell,N}) = \frac{1}{N}$ , for any  $\ell \in \{1, \dots, N\}$  and  $\epsilon > 0$ , Chebyshev’s inequality implies

$$\Pr \{|J_{\ell,N} - 1/N| \geq \epsilon\} \leq \frac{\text{Var}(J_{\ell,N})}{\epsilon^2},$$

where,  $Var_{F_1^{pri}}(J_{\ell,N}) = \frac{N-1}{N^2(a+1)}$ . Assuming  $a = \kappa^2 c$  for  $\kappa \in \{0, 1, \dots\}$  and a fixed positive number  $c$ , gives

$$\Pr \{|J_{\ell,N} - 1/N| \geq \epsilon\} \leq \frac{1}{\kappa^2 c \epsilon^2}.$$

The convergence of series  $\sum_{\kappa=0}^{\infty} \kappa^{-2}$  implies  $\sum_{\kappa=0}^{\infty} \Pr \{|J_{\ell,N} - 1/N| \geq \epsilon\} < \infty$ . By letting  $a \rightarrow \infty$ , the first Borel Cantelli lemma concludes  $|J_{\ell,N} - 1/N| \xrightarrow{a.s.} 0$  and the result of (i) follows. To prove (i), it is enough to show  $\Pr \{\lim_{a \rightarrow \infty} (J_{\ell,N} J_{t,N}) \neq \frac{1}{N^2}\} = 0$ . To prove this for the probability space  $(\Omega, \mathcal{F}, \Pr)$ , let

$$A = \left\{ \omega \in \Omega : \lim_{a \rightarrow \infty} (J_{\ell,N}(\omega) J_{t,N}(\omega)) \neq \frac{1}{N^2} \right\}, \quad B = \left\{ \omega \in \Omega : \lim_{a \rightarrow \infty} (J_{\ell,N}(\omega)) \neq \frac{1}{N} \right\},$$

$$C = \left\{ \omega \in \Omega : \lim_{a \rightarrow \infty} (J_{t,N}(\omega)) \neq \frac{1}{N} \right\},$$

where,  $\Pr(B)$  and  $\Pr(C)$  are zero by (i). Since  $A \subseteq B \cup C$ , then,

$$1 - \Pr \left\{ \omega \in \Omega : \lim_{a \rightarrow \infty} (J_{\ell,N}(\omega) J_{t,N}(\omega)) = \frac{1}{N^2} \right\} = \Pr(A) \leq \Pr(B) + \Pr(C) = 0,$$

which concludes the result. ■

## B. Hypothesis Testing Evaluation

---

**Algorithm 3** Pseudocode of plotting ROC and computing AUC in semi-BNP test

---

- 1: Initialize  $a$ ,  $N$ ,  $\ell$ , and  $M$ .
- 2:  $r \leftarrow 100$
- 3:  $RB^\dagger | \mathcal{H}_0 \leftarrow$  Compute  $RB$  for  $r$  sample of sizes  $n$  generated under the null hypothesis.
- 4:  $RB | \mathcal{H}_1 \leftarrow$  Compute  $RB$  for  $r$  sample of sizes  $n$  generated under the alternative hypothesis.
- 5:  $T \leftarrow$  A sequence of numbers between 0 to  $20^\ddagger$  with length  $L$ . ▷ The discrimination threshold for the semi-BNP test.
- 6:  $TP \leftarrow$  A vector whose each component represents the number of components of the vector  $RB | \mathcal{H}_1$  which is less than each component of  $T$ .
- 7:  $FN \leftarrow$  A vector whose each component represents the number of components of the vector  $RB | \mathcal{H}_1$  which is greater than each component of  $T$ .
- 8:  $FP \leftarrow$  A vector whose each component represents the number of components of the vector  $RB | \mathcal{H}_0$  which is less than each component of  $T$ .
- 9:  $TN \leftarrow$  A vector whose each component represents the number of components of the vector  $RB | \mathcal{H}_0$  which is greater than each component of  $T$ .
- 10: Compute the confusion matrix as:

$$\begin{pmatrix} TNR := \frac{TN}{TN+FP} & FNR := \frac{FN}{FN+TP} \\ \text{(1-Type I error)} & \text{(Type II error)} \\ FPR := \frac{FP}{FP+TN} & TPR := \frac{TP}{TP+FN} \\ \text{(Type I error)} & \text{(1-Type II error)} \end{pmatrix}.$$

- 11: ROC  $\leftarrow$  Drawing a linear plot of  $TPR$  against  $FPR$ .
- 12: AUC  $\leftarrow$  Computing the area under the ROC.

13: **return** ROC and AUC.

<sup>†</sup> It should be changed to the  $p$ -value in the FNP test.

<sup>‡</sup> It should be changed to 1 in the FNP test.

---